GluK1 kainate receptors are necessary for functional maturation of parvalbumin interneurons regulating amygdala circuit function

Joni Haikonen*, Rakenduvadhana Srinivasan*, Simo Ojanen, Maria Ryazantseva, Gabija Zumaraite and Sari E. Lauri#

* equal contribution

corresponding author

HiLife Neuroscience Center and Molecular and Integrative Biosciences Research Programme, University of Helsinki, Finland

Abstract

Parvalbumin expressing (PV+) interneurons are key players in the local inhibitory circuits and their developmental maturation coincides with the onset of adult-type network dynamics in the brain. Glutamatergic signaling regulates emergence of the unique PV+ neuron phenotype, yet the receptor mechanisms involved are not fully understood. Here we show that GluK1 subunit containing kainate receptors (KARs) are necessary for development and maintenance of the neurochemical and functional properties of PV+ interneurons in the basolateral amygdala (BLA). Ablation of GluK1 expression specifically from PV+ neurons resulted in low parvalbumin expression and loss of their characteristic high firing rate throughout development. In addition, we observed reduced spontaneous excitatory synaptic activity at adult GluK1 lacking PV+ neurons. Intriguingly, knockdown of GluK1 expression from adult PV+ neurons was sufficient to abolish the PV+ phenotype, suggesting a role for GluK1 in dynamic regulation of PV+ neuron maturation state. The PV+ neuron dysfunction in the absence of GluK1 perturbed feedforward inhibition and long-term potentiation (LTP) in the BLA and resulted in developmentally originating changes in the glutamatergic connectivity. Behaviorally, the absence of GluK1 from PV+ interneurons associated with hyperactivity and increased fear of novelty. These results indicate a critical role for GluK1 KARs in regulation of PV+ interneuron function across development and suggest GluK1 as a potential therapeutic target for pathologies involving PV+ neuron malfunction.

Introduction

Kainate receptors (KARs) are glutamate receptors with both ionotropic and metabotropic modes of action, composed of tetrameric arrangements of GluK1-5 subunits. They are widely expressed in both glutamatergic and GABAergic neurons, in pre- and postsynaptic terminals, to modulate synaptic transmission and plasticity (reviewed by Pinheiro & Mulle, 2006; Lerma & Marques, 2013; Nair et al., 2021). In addition, KARs are highly expressed during early postnatal development and significantly contribute to circuit development (Lanore et al., 2012; Ryazantseva et al., 2020; reviewed by Lauri et al., 2021). Accordingly, KARs malfunction has been implicated in various neurodevelopmental and psychiatric disorders, as well as in epilepsy (Jane et al., 2009; Valbuena and Lerma 2021; Mulle and Crepel, 2021). Although most of the physiological functions described for KARs in the developing circuitry are related to glutamatergic transmission, GluK1 subunit containing KARs, in particular, are also implicated in development and maturation of GABAergic interneurons and GABAergic synaptic transmission (Segerstrale et al., 2010; Orav et al., 2019; Jack et al., 2019; Ojanen et al., 2023); however, their contribution to differentiation of various interneuron subtypes remains unknown.

Parvalbumin (PV+) expressing neurons represent a prominent subtype of GABAergic interneurons in the brain with unique physiological properties that enable them to control local network dynamics (Hu et al., 2014). These interneurons reach their full electrophysiological and morphological maturity relatively late in development which, along with acquisition of extracellular components, such as perineuronal nets (PNNs), close off the early critical period of plasticity (Hensch, 2005; Gibel-Russo et al., 2022). Glutamatergic synaptic input is essential for activity-dependent maturation of interneurons (De Marco García et al., 2015; Dehorter et al., 2015; Wamsley & Fishell, 2017). Of the various glutamate receptor subtypes, NMDA receptor mediated signaling has been shown to profoundly influence development and adult functions of the PV+ neurons (Korotkova et al., 2010; Mahadevan et al., 2021; Pafundo et al., 2021). PV+ neurons also contain KARs (Englund et al., 2021; Wyeth et al., 2017) yet their roles in regulating PV+ neuron specific functions are not well characterized.

We have recently shown that GluK1 subunit containing KARs regulate the excitability of PV+ neurons and consequently, the function of the local disinhibitory circuit in the basolateral amygdala (BLA) (Englund et al., 2021). Furthermore, early life stress (ELS), involving alterations

in neurochemical maturation of PV+ neurons (reviewed by Guadagno et al., 2021), associates with downregulation of GluK1 expression in BLA PV+ neurons (Englund et al., 2021). Altogether, these data suggest that KARs are in a crucial position to orchestrate interplay between glutamatergic and GABAergic systems and to drive activity-dependent maturation of PV+ neurons.

In the present work, we used genetic tools to eliminate GluK1 expression selectively in PV+ interneurons, to study the role of GluK1 KARs on PV+ interneuron development and function, as well as its broader significance on the BLA circuitry and behavior. We show that GluK1 expression is essential for the maturation and maintenance of the PV+ neuron phenotype. Loss of GluK1 in the PV+ interneurons associates with robust reduction in PV expression and PV+ neuron excitability and affects feedforward inhibition and synaptic plasticity in the BLA. The amygdala circuit dysfunction observed in the mice where GluK1 was selectively ablated in the PV+ interneurons associated with behavioral changes, including hyperactivity and fear of novelty.

Taken together, these results provide vital new evidence for the critical role of GluK1 KARs in the development and maturation of PV+ interneurons, with potential implications to the variety of neurodevelopmental disorders involving perturbed PV+ neuron function

Materials and methods

Animal models: Experiments were performed using males and females between postnatal day (P) 4-70 of the following mouse lines: a conditional (floxed) line for GluK1 (*Grik1*$^{tm1c/tm1c}$; Ryazantseva et al., 2020) and PV-Cre (JAX: 008069). PV-Cre mice were crossed with Ai14 (JAX 007914) to produce PV-TdTomato reporters and with *Grik1*^{tm1c} to produce mice lacking *Grik1* selectively in PV+ interneurons (*Grik1*$^{tm1d/tm1d}$; from here on *PV-Grik1*$^{-/-}$). All mice were in the C57BL/6J background. Mice were group housed (2–5 animals of the same sex/cage) in a temperature and humidity-controlled environment, with a 12/12h light/dark cycle and *ad libitum* access to food and water. The animals were sacrificed for experiments between 9 a.m. and 3 p.m., during the light period (lights on 6 a.m., off 6 p.m.). The stage of the estrous cycle was not controlled. All experiments were done in accordance with the University of Helsinki Animal Welfare Guidelines and approved by the Animal Experiment Board in Finland.

Stereotaxic surgery and viral vectors:

AAV serotype 8 viral vectors encoding for floxed EGFP under the synapsin promoter (pAAV-hSyn-DIO-EGFP (#50457)) were purchased from Addgene. rAAV-PV-EGFP-bGH polyA and rAAV-PV-CRE-EGFP-bGH polyA encoding for EGFP under the PV promoter were purchased from BrainVTA, Wuhan, China. Following craniotomical surgery, AAVs were stereotaxically injected into the BLA of adult mice under anesthesia as previously described (Englund et al., 2021). The following coordinates were used: (1) from bregma AP −1,7 ML 3.2-3.3 DV 4.3 and 4.2 (2) from bregma AP −2.2 ML 3.2-3.3 DV 4.3 and 4.2. 150 nl of viral particles were delivered to each injection site and brain slice electrophysiological experiments were carried out 2-3 weeks following the injections.

For experiments with the juvenile cohorts, viral injections were done on neonates (P4-6) using a non-invasive method (without surgical incisions of the scalp) with minimal anesthesia, to ensure survival of pups. Viral particles were directly injected through scalp and cranium using a stainless-steel needle (33 ga. beveled NanoFil needle, WPI). Stereotaxic coordinates were calculated from the eyes (due to bregma not being visible through the scalp) and the following coordinates were used from eyes: for P4 animals: AP-2.6, ML-4.5, DV-2.4, 3. For P6 animals: AP-2.6, ML-4.6, DV-2.5, 3. Brain slice electrophysiological experiments were conducted 10-12 days post viral injections.

After viral injection surgeries, the adult mice were individually housed to prevent accidental opening of sutures and exacerbation of surgical wounds due to fighting. The injected neonates were housed with the dams with a 100% survival rate owing to the absence of surgical wounds.

Slice preparation for electrophysiological recordings. 2–3-month-old mice were anesthetized with isoflurane and quickly decapitated. The brain was extracted and immediately placed in carbogenated (95% O_2/5%CO_2) ice-cold *N*-Methyl-D-glucamine (NMDG) based protective cutting solution (pH 7.3-7.4) containing (in mM): 92 NMDG, 3 Na-pyruvate, 5 Na L-ascorbate, 2 thiourea, 20 HEPES, 30 $NaHCO_3$, 25 glucose 1.25 NaH_2PO_4, 2.5 KCl, 0.5 $CaCl_2$ and 10 $MgSO_4 \cdot 7H_2O$ (300-310 mOsm). For recording of virally transduced interneurons the mice were transcardially perfused with ice-cold NMDG solution prior to decapitation. The cerebellum and a small part of the prefrontal cortex were trimmed off, the brain glued to a stage and transferred to a vibratome (Leica VT 1200S) to obtain 300 µm thick brain slices. Slices containing the amygdala

were placed into a slice holder in 34ºC heat bath, containing the NMDG protective solution. Slices were incubated in the heat bath for 8-12 minutes and transferred into a separate slice holder in room temperature filled with oxygenated HEPES-based storing solution containing (in mM): 92 NaCl, 3 Na-pyruvate, 5 Na L-ascorbate, 2 thiourea, 20 HEPES, 30 $NaHCO_3$, 25 glucose, 1.25 NaH_2PO_4, 2.5 KCl, 2 $CaCl_2$ and 2 $MgSO_4 \cdot 7H_2O$ (300-310 mOsm).

Juvenile mice (P16-21) animals were brought from housed cages 5 minutes prior to decapitation to minimize stress due to maternal separation and anaesthetized using isoflurane. Following rapid decapitation and opening of the cranium, the brain was placed immediately into ice-cold sucrose-based sectioning solution of the following composition: 87 mM NaCl, 2.5 mM KCl, 0.5 mM $CaCl_2$, 25 mM $NaHCO_3$, 1.25 mM NaH2PO4, 7 mM $MgSO_4$, 75 mM sucrose and 25 mM D-glucose (300-310 mOsm). 250 µM thick coronal slices were cut in the same manner as adults and the slices recovered for 1h in ACSF containing (in mM): 124 NaCl, 3 KCl, 1.25 NaH_2PO_4, 26 $NaHCO_3$, 15 glucose, 1 $MgSO_4$. $7H_2O$, 2 $CaCl_2$ (~ 300-310 mOsm) at 34ºC. All steps were performed with continuous carbogen bubbling.

Electrophysiological recordings. After 1–6h of recovery, the slices were placed in a submerged heated (32–34°C) recording chamber and perfused with standard carbogenated ACSF containing (in mM): 124 NaCl, 3 KCl, 1.25 NaH_2PO_4, 26 $NaHCO_3$, 15 glucose, 1 $MgSO_4$. $7H_2O$, 2 $CaCl_2$ (300-310 mOsm) at the speed of 1–2ml/min. Whole-cell patch-clamp recordings were done from BLA neurons under visual guidance using patch electrodes with resistance of 2–7 MΩ. Multiclamp 700B amplifier (Molecular Devices), Digidata 1322 (Molecular Devices) or NI USB-6341 A/D board (National Instruments) and WinLTP version 2.20 (Anderson & Collingridge, 2007) or pClamp 11.0 software were used for data collection, with low pass filter (10 kHz) and sampling rate of 20 kHz. In all voltage-clamp recordings, uncompensated series resistance (Rs) was monitored by measuring the peak amplitude of the fast whole-cell capacitive current in response to 5 mV step. Only experiments where Rs <30 MΩ, and with <20% change in Rs during the experiment, were included in analysis.

Current clamp recordings of intrinsic excitability. Whole cell recordings to characterize intrinsic excitability were done with a pipette solution of the following composition (in mM): 135 K-gluconate, 10 HEPES, 5 EGTA, 2 KCl, 2 $Ca(OH)_2$, 4 Mg-ATP, 0.5 Na-GTP, (280 mOsm, pH 7.2). Current steps of 500 ms duration and of varying amplitude (-100 to 400 pA with 25 pA increments)

were injected to probe firing frequency, along with passive-membrane properties such as input resistance. All cells were held at resting membrane potential. Action potential (AP) half-width and amplitude of the afterhyperpolarizing potential (AHP) are analyzed from the 3rd spike in the train using Clampfit software.

Spontaneous excitatory postsynaptic currents (sEPSC,) were recorded from PV+ interneurons with the K-gluconate based pipette filling solution, following completion of current clamp recordings. The membrane potential was clamped at -70 mV and sEPSCs were recorded for 15 minutes.

Spontaneous excitatory and inhibitory postsynaptic currents (sEPSC, sIPSC) were recorded using a cesium-based pipette filling solution (pH 7.2, 280 mOsm) containing (in mM): 125.5 Cs-methanesulfonate, 10 HEPES, 5 EGTA, 8 NaCl, 5 QX314, 4 Mg-ATP, 0.3 Na-GTP. The membrane potential was first clamped at -70 mV and sEPSCs were recorded for 10 min. Afterwards, the membrane potential was slowly raised to 0 mV, the reversal potential of glutamatergic currents, in order to measure sIPSCs.

Spontaneous miniature postsynaptic currents (mEPSC) were recorded from BLA neurons using the cesium-based filling solution supplemented with 0.3% Biocytin, for later morphological analysis of spines. 1 µM of tetrodotoxin (TTX) was added to the perfusion solution. The membrane potential was first clamped at -70 mV and mEPSCs were recorded for 20-30 min.

Analysis of the spontaneous synaptic events was done manually using Minianalysis program 6.0.3. EPSCs and IPSCs were identified as inward and outward currents, respectively, with typical kinetics, that were at least 3 times the amplitude of the baseline level of noise. 5 minutes of recording / cell was analyzed.

Evoked glutamatergic and GABAergic (EPSC, dIPSC) responses were recorded using the cesium-based filling solution. EPSCs and dIPSCs were evoked with a bipolar stimulation electrode (nickel-chromium wire), placed in the external capsule to stimulate cortical inputs coming to the amygdala every 20 sec during the recording. The membrane potential was first held at -70 mV to record 5 min of EPSCs, after which, the cell was slowly depolarized to 0 mV to record 10-20 min of dIPSC. 10 µM CNQX was added at the end of the recording to confirm the disynaptic nature of the response (> 80% block of the IPSC amplitude). Excitation/inhibition balance analysis was done

using WinLTP software, averaging 5 min of evoked responses and then calculating the EPSC/dIPSC amplitude ratio. For experiments probing the effect of ACET on EPSCs and paired pulse (50 ms interval) ratios, a 15-minute baseline was recorded, following which 200 nM ACET was applied for 10 minutes with a consequent washout. 2-exponential fit for the EPSC decay was done using Clampfit software to separate the fast and slow components of the synaptic response.

Field recordings were done using an interface chamber (32–34ºC). In order to obtain stable recordings, slices were allowed to acclimate to the conditions of the recording chamber for >30 minutes before the experiment was started. fEPSPs were evoked with a bipolar stimulation electrode (nickel-chromium wire) placed in the external capsule to mimic activation of cortical inputs, while the recording electrode (resistance 1–3 MΩ, filled with standard ACSF) was placed in the lateral amygdala (LA). The stimulation intensity was adjusted to produce a half-maximal response size. After a stable baseline, LTP was induced using theta-burst stimulation (TBS) (6 bursts of 8/100 Hz at 5 Hz), repeated 3 times with 5 min intervals. After TBS, synaptic responses were recorded for 60 min. Analysis was done using the WinLTP software, averaging 3 responses per timepoint. Averages to evaluate the level of synaptic potentiation were calculated over a stable 10 min period, just before TBS and at the end of the recording.

Immunohistochemistry. For parvalbumin (PV), P21 and P60 mice were intracardially perfused with PBS and 4% PFA under deep anesthesia. The brains were carefully extracted and placed in 4% PFA overnight at 4ºC, after which they were washed twice with PBS. 40 µM thick coronal sections were cut using a vibratome (Leica VT 1200S) and placed in 12-well well plates. The sections were incubated in a blocking solution (10% goat serum, 1% BSA and 0.5% Triton-X in PBS), in room temperature (RT), for 1h, after which they were washed with a wash buffer (1% goat serum, 1% BSA and 0.5% Triton-X in PBS) for 20 min in RT. The sections were incubated in primary antibodies diluted into the wash buffer (1:1000 PV 235 mouse (SWANT)) overnight in 4ºC. The next day, the sections were washed with the wash buffer 2 x 20 min in RT, followed by incubation in secondary antibodies diluted into the wash buffer (1:1000 Alexa 488 goat anti-mouse (Life Technologies)) in RT. The sections were washed with PBS 3 x 20 min in RT, after which they were mounted on to microscope slides using Vectashield mounting medium. The stained sections were imaged with Zeiss Axio Imager.M2 microscope equipped with ApoTome 2 structured illumination slider, using PlanApo ×10 objective and CMOS camera (Hamamatsu

ORCA Flash 4.0 V2) and Zen Blue software. All sections were imaged with the same exposure time for integrated optical density (IOD) analysis. The density and IOD of stained cells within BLA was calculated using ImageJ software.

Spine density analysis was done *post hoc* for biocytin filled amygdala neurons. Sections were fixed overnight in 4% PFA in 4°C, washed with PBS and placed in a permeabilization solution (0.3% Triton-X in PBS) overnight in 4°C. Next, 1:500 streptavidin Alexa 568 (Life Technologies) was added (overnight in 4°C), after which the sections were mounted on microscope slides using ProLong™ Gold Antifade Mountant (Thermofisher). Dendritic spines were imaged using a LSM Zeiss 710 confocal microscope (alpha Plan146 Apochromat 63x/1.46 OilKorr M27 objectives) with resolution of 15.17 pixels/µm and Z-stack interval of 0.5 µm. Spine density was calculated from the first branch (length 60-100 µm) of the dendritic tree. All analysis was done manually using ImageJ software.

Behavioral tests

Elevated plus-maze (EPM). The maze consisted of two open arms (30 x 5 cm) and two enclosed arms (30 x 5 cm) connected by central platform (5 x 5 cm) and elevated to 40 cm above the floor. Open arms were surrounded by 0.5 cm high edges to prevent accidental falling of mice. The floor of each arm was light grey and the closed arms had transparent (15 cm high) side- and end-walls. The illumination level in all arms was ~150 lx. The animal was placed in the center of the maze facing one of the closed arms and observed for 5 minutes. The trials were recorded with Ethovision XT13 videotracking software (Noldus Information Technology, Wageningen, The Netherlands) to measure the time spent in different zones of the maze.

Open field (OF). The mice were released in the corner of novel open field arena (white floor, transparent walls, 30 x 30 cm, Med Associates). Horizontal activity was recorded by infrared sensors during 30 minutes (light intensity ~150 lx). Peripheral zone was defined as a 6 cm wide corridor along the wall.

Fear conditioning (FC). The experiments were carried out employing a computer-controlled fear conditioning system (TSE Systems, Germany). Training was performed in a transparent acrylic cage (23 × 23 × 35 cm) within a constantly illuminated (~ 100 lx) fear conditioning box. A loudspeaker provided a constant, white background noise (68 dB) for 120 s followed by 10 kHz

tone (CS, 76 dB, pulsed 5 Hz) for 30 s. During conditioning, the tone was terminated by a footshock (US, 0.6 mA, 2 s, constant current) delivered through a stainless steel grid-floor (bar Ø 4 mm, distance between the bars 10 mm). Two CS-US pairings were separated by a 30 s pause. Contextual memory was tested 24 h after the training. The animals were returned to the conditioning box and total time of freezing (defined as an absence of any movements for more than 2 s) was measured through infrared light beams scanned continuously with a frequency of 10 Hz. The CS was not used during this time. Memory for the CS (tone) was tested 2 h later in a novel context. The new context was a similarly sized acrylic box with black non-transparent walls and smooth floor. A layer of wood chips (clean bedding material) under the floor provided a novel odour to the chamber. After 120 s of free exploration in a novel context the CS was applied for additional 120 s and freezing was measured as above.

Statistical analysis. All statistical analyses were done on raw (not normalized) data using Sigma Plot or Prism GraphPad software. The sample sizes were based on previous experience on similar experiments. All data were first assessed for normality and homogeneity of variance and the statistical test was chosen accordingly. Differences between two groups were analyzed using two-tailed t-test, Mann–Whitney rank-sum test, one-way ANOVA, one-way repeated measures ANOVA, or mixed effects model (REML), as appropriate. Two-way ANOVA with Holm–Sidak post-hoc comparison was used to compare effects of sex and genotype or age and genotype. For data that were not normally distributed, one-way ANOVA on ranks (Kruskal Wallis) test was used for post-hoc comparison. The results were considered significant when $p < 0.05$. All the pooled data are given as mean ± SEM.

Results

GluK1 subunit containing KARs contribute to glutamatergic synaptic transmission to PV+ interneurons in the juvenile BLA

Our previous research has shown the presence of functional GluK1 subunit containing KARs in PV+ interneurons in the adult mouse BLA (Englund et al., 2021). To confirm the presence of GluK1 KARs in PV+ interneurons also in the developing amygdala, we recorded evoked

excitatory post synaptic currents (EPSCs) from PV+ cells of 16-18 day old PV-Tdtomato mice, and investigated their sensitivity to ACET, an antagonist selective for GluK1 subunit containing receptors (Dargan et al., 2009). Since previous work examining the effect of ACET on adult PV+ cells did not reveal any sex differences (Englund et al., 2021), we focused on males for this data set. Application of (200 nM) ACET resulted in significant reduction in the EPSC amplitude ($p = 0.0002$, paired t-test), evoked by stimulation of cortical afferents, without affecting the paired-pulse ratio (Figure 1A, B). We also used 2-exponential fit to analyze separately the amplitudes of the fast (AMPA-receptor mediated) and slow components of the EPSC. The amplitude of the slow decaying component of the eEPSC was also significantly reduced in the presence of ACET ($p = 0.0027$, paired t-test). These data indicate that postsynaptic GluK1 containing KARs regulate glutamatergic drive onto PV+ interneurons and contribute to the EPSC.

GluK1 regulates parvalbumin expression and the density of PV+ interneurons in the BLA

Glutamatergic input is critical for driving development and maturation of the PV+ neuron phenotype (Korotkova et al. 2010; De Marco García et al. 2015; Mahadevan et al. 2021). Having confirmed that GluK1 KARs contribute to synaptic transmission to PV+ interneurons in the BLA already at juvenile stage, we investigated how the absence of GluK1 in PV+ interneurons affects their maturation via immunohistochemistry at two time points, P21 and P60. We used a conditional knockout mouse line lacking GluK1 KAR expression selectively in PV+ interneurons (*PV-Grik1*$^{-/-}$) to study how elimination of GluK1 expression affects PV+ cell density and the intensity PV labelling, commonly used as a measure of PV+ cell neurochemical maturation (Figure 2A). Analysis of PV+ cell density in the BLA of male mice indicated that there was a significant effect of genotype ($F_{(1, 11)} = 46.951$, $p < 0.001$, 2-way ANOVA) but not age ($F_{(1, 11)} = 1.998$, $p = 0.195$, 2-way ANOVA). Post-hoc comparison revealed that PV+ cell density was lower in both adult and juvenile *PV-Grik1*$^{-/-}$ as compared to controls (Figure 2A). In addition, there was a significant effect of age ($F_{(1, 11)} = 31.985$, $p < 0.001$, 2-way ANOVA) and genotype ($F_{(1, 11)} = 129.053$, $p < 0.001$, 2-way ANOVA) on intensity optical density (IOD) of PV labeling. Post-hoc comparisons revealed that PV+ cell IOD was significantly lower in both adult and juvenile *PV-Grik1*$^{-/-}$ mice, as compared to their respective controls (Figure 2A).

Next, we wanted to see whether a local viral knockdown of GluK1 in PV+ cells in adulthood is sufficient to produce the perturbed PV phenotype. To this end, we infected the BLA of a conditional (floxed) mouse line for GluK1 (*Grik1*^{tm1c}) with AAV viral vectors encoding for either PV-EGFP (control) or PV-CRE-EGFP (*PV-Grik1* KD) and stained them for PV. Since the specificity of the viruses for PV+ neurons was less than ideal (% of EGFP-positive PV+ cells, PV-EGFP: 11.81 ± 1.74%, PV-CRE-EGFP: 58.42 ± 3.25 %), only EGFP-positive PV+ cells were selected for IOD analysis. Mice infected with PV-CRE-EGFP had significantly lower PV+ cell density ($F_{(1, 28)} = 5.544$, $p = 0.026$) and IOD in the EGFP-positive PV+ cells ($F_{(1, 86)} = 38.845$, $p < 0.001$) in the BLA as compared to controls (Figure 2B and C).

Taken together, these results show that GluK1 KARs profoundly affect maturation of the PV+ cells in the BLA.

GluK1 is necessary for the high-frequency firing phenotype of PV+ interneurons in the BLA

Having observed the profound neurochemical alterations in our immunohistochemical experiments, we set out to investigate whether absence of GluK1 expression affected physiological functions of PV+ interneurons. For this, we began with current clamp whole cell recordings of PV+ interneurons in adult BLA to investigate their excitability in response to depolarizing current steps. The experiments revealed that PV+ cell excitability was significantly lower in the *PV-Grik1*$^{-/-}$ mice in comparison to controls (*PV-Cre* mice). This was reflected in their maximal firing frequency as well as firing frequency at every step size, observed in both the sexes of adult mice ($p < 0.0001$, mixed effects model REML test) (Figure 3A, Supplementary Figure 1A), consistent with a loss of their characteristic high frequency firing phenotype. Furthermore, in the adult *PV-Grik1*$^{-/-}$ mice, the rheobase of the PV+ interneurons was significantly higher ($p = 0.0088$, Mann Whitney test) and input resistance was lower ($p = 0.0007$, Mann-Whitney test) than in controls, while resting membrane potential remained the same across both the groups and sexes (Figure 3C).

Next, we investigated if a local knockdown of GluK1 expression in adulthood is sufficient to produce this profound loss of PV+ cell excitability. Since the loss of excitability was seen in both males and females in the *PV-Grik1*$^{-/-}$ adults, we focused only on males for the *PV-Grik1* KD dataset. Given that the viral vectors were not fully specific to PV+ neurons, we used additional

criteria to exclude prospective principal neurons. First, only those neurons having a somatic diameter of less than 15 μm, that were spherical or fusiform in appearance, were selected for recordings under visual guidance (Braga et al., 2009; Rainnie et al., 2006). Furthermore, cells with action potential halfwidth >1 ms, and spike frequency adaptation (spike interval ratio < 0.7, for 1st-2nd / 2nd-3rd AP), were excluded at the analysis stage (representing 17 % of recorded neurons) (Faber et al., 2001; Mahanty & Sah, 1998).

PV-Grik1 KD cells displayed low excitability, similar to that seen in the *PV-Grik1*$^{-/-}$ mice. In *PV-Grik1* KD cells, the maximal firing frequency and firing frequency at every stimulation intensity was significantly lower than in controls ($p < 0.0001$, mixed effects model REML test, Fig 3E). *PV-Grik1* KD cells also had a significantly lower input resistance ($p = 0.0228$, Mann Whitney test, Fig 3) than controls. Although there was a trend of higher rheobase values in the *PV-Grik1* KD vs control PV+ neurons, this was not statistically significant and resting membrane potentials were unaffected (Supplementary Fig. 1C).

To examine whether the loss excitability in GluK1 lacking PV+ cells is already present during development, we conducted similar current clamp whole cell recordings of BLA PV+ interneurons from 16-18 day old *PV-Grik1*$^{-/-}$ mice. Our experiments revealed that in both males and females, the firing frequency of PV+ neurons was significantly lower in *PV-Grik1*$^{-/-}$ mice as compared to controls ($p < 0.0001$ Mixed-effects model (REML)) (Figure 3B). The effect of GluK1 elimination on PV+ neuron excitability was less prominent in juvenile females (Supplementary Figure 1B), possibly because of a difference in developmental trajectories and timings between sexes. Moreover, we observed higher rheobase ($p = 0.0069$, Mann Whitney) and lower input resistance ($p < 0.0001$, Mann Whitney), across both sexes in *PV-Grik1*$^{-/-}$ PV+ neurons (Figure 3D).

For further insight on the active membrane properties of PV+ neurons, we also compared action potential (AP) half width and the amplitude of the after hyperpolarization (AHP) between the genotypes. The AP-halfwidth is a parameter shown to decrease in PV cells as a consequence of development, accompanying the augmentation of their firing rate (Doischer et al., 2008; Goldberg et al., 2011). Accordingly, we observed a significant decrease in AP halfwidth in the control PV+ neurons from juvenile to adult stage ($p < 0.0001$, Mann-Whitney test, supplementary Fig 1A). In adult *PV-Grik1*$^{-/-}$ PV+ neurons, but not at the juveniles, the AP-halfwidth was significantly higher as compared to controls ($p = 0.0410$, Mann Whitney test; Figure 3C), suggesting impaired

maturation of PV cells. Indeed, there was no difference in AP halfwidth between juvenile and adult *PV-Grik1*$^{-/-}$ PV+ neurons of either sex ($p = 0.2155$, Mann-Whitney test, supplementary Fig 1A). In addition, we observed that AP-halfwidth was higher in the adult *PV-Grik1* KD cells as compared to controls ($p = 0.0146$, Mann Whitney test, Fig 3E), suggesting that GluK1 KARs play a vital role in maintaining the fast action potential kinetics of adult PV+ cells.

After-hyperpolarization (AHP) current is an electrophysiological signature that distinguishes PV+ cells from other interneurons (Ascoli et al., 2008; DeFelipe et al., 2013; Hu et al., 2014a; Tremblay et al., 2016; Nahar et al., 2021). Our experiments revealed that the amplitude of the AHP current was significantly lower in both, adult and juvenile *PV-Grik1*$^{-/-}$ PV+ neurons of both sexes ($p = 0.0006$, two tailed t test and $p = 0.0332$, Kolmogorov-Smirnov test, respectively) but not significantly lower in *PV-Grik1* KD neurons, as compared to their respective controls (Figure 3C, D & E).

These results clearly indicate the crucial role of GluK1 in maintaining PV+ cell excitability and electrophysiological characteristics across development. Furthermore, these results also reveal a role for GluK1 in maintaining the characteristic PV+ electrophysiological phenotype (such as the high frequency firing) in the adult stage, beyond the developmental windows of plasticity.

GluK1 ablation perturbs glutamatergic inputs to PV+ interneurons

We next examined whether absence of GluK1 affected glutamatergic input to PV+ cells by conducting whole cell voltage clamp recordings of spontaneous excitatory postsynaptic currents (sEPSCs). These recordings revealed significantly lower frequency and amplitude of sEPSCs in the adult *PV-Grik1*$^{-/-}$ PV+ cells as compared to controls, across both sexes ($p = 0.0005$, Mann Whitney test and $p=0.0004$, two-tailed t test, respectively)(Figure 4A). Interestingly, while the sEPSC frequency was affected in both sexes, the amplitude of sEPSCs was lower in *PV-Grik1*$^{-/-}$ females ($p < 0.0001$, two tailed t test), but not in males (Supplementary Figure 2). Similar changes in glutamatergic input to PV+ interneurons were also observed in the adult *PV-Grik1* KD neurons. The sEPSC frequency, but not the amplitude was significantly lower in *PV-Grik1* KD neurons in comparison to controls ($p = 0.0003$, Mann Whitney) (Figure 4C). In these recordings, putative

principal neurons were excluded from the analysis using the same electrophysiological criteria as defined for the data in figure 3.

Interestingly, in contrast to the adults, sEPSC frequency was significantly higher in the juvenile (P16-18) *PV-Grik1*$^{-/-}$ neurons as compared to controls, in both sexes (males: $p = 0.0098$, females: $p = 0.0153$, Mann Whitney and Kolmogorov-Smirnov tests, respectively) (Figure 4B). sEPSC amplitudes were not different between the groups.

These data indicate the GluK1 expression in the adult stage is necessary to maintain glutamatergic input to PV+ neurons. In juveniles this effect was not observed, possibly because of efficient homeostatic compensatory mechanisms during the early plasticity window.

Elimination of GluK1 in PV+ interneurons affects development of the synaptic circuitry in the BLA

Since the absence of GluK1 KARs in PV+ interneurons led to profound alterations in their neurochemical and functional maturation, we next investigated the broader consequences of this on BLA circuitry by recording the excitability and synaptic inputs in BLA principal neurons (PNs). We decided to focus our efforts solely on males, as the changes in PV+ cell excitability, AP kinetics and membrane properties in *PV-Grik1*$^{-/-}$ mice were similar in both sexes. The firing frequency of the adult BLA PNs in response to depolarizing steps was not different between the control and *PV-Grik1*$^{-/-}$ groups ($F_{(1, 131)} = 0.9559$, $p = 0.33$, mixed effects model (REML); Figure 5A). Also, we detected no differences between the genotypes ($F_{(1, 46)} = 0.247$, $p = 0.62$, 2-way ANOVA) in the ongoing GABAergic inhibition in either age group, when assessed by spontaneous inhibitory postsynaptic currents (sIPSC)($F_{(1, 46)} = 0.236$, $p = 0.63$, 2-way ANOVA) (Figure 5B). Interestingly, however, there was a significant genotype effect on the frequency of sEPSCs, reflecting the ongoing glutamatergic input to BLA PNs ($F_{(1, 45)} = 14.886$, $p < 0.001$, 2-way ANOVA). Post-hoc comparisons revealed that sEPSC frequency in *PV-Grik1*$^{-/-}$ mice was significantly lower in adult animals, when comparing to controls (Figure 5B). In juvenile animals, sEPSC frequency was markedly lower but this effect did not reach statistical significance (Figure 5B). No differences between the genotypes were detected in sEPSC or sIPSC amplitudes, either in adult or juvenile mice (adult: sEPSC: $p = 0.074$, one-way ANOVA on ranks; sIPSC: $F_{(1, 20)} =$

0.0677, p = 0.798, one-way ANOVA; juvenile: sEPSC: $F_{(1,24)}$ = 0.652, p = 0.428, one-way ANOVA; sIPSC: p = 0.192, one-way ANOVA on ranks) (Supplementary Figure 2).

Thus, despite the robust loss of PV+ neuron excitability in the absence of GluK1 expression, the main effect observed in principal neurons in PV-*Grik1*$^{-/-}$ mice was a paradoxical decrease in glutamatergic input. Next, we investigated whether this intriguing reduction in glutamatergic drive onto BLA PNs in PV-*Grik1*$^{-/-}$ was driven by changes in network excitability or reflected altered glutamatergic connectivity. To this end, we recorded miniature excitatory postsynaptic currents (mEPSCs) from adult BLA PNs, while simultaneously filling the cells with biocytin for *post hoc* spine morphological analysis. mEPSC frequency and amplitude were not significantly different between the genotypes (frequency: $F_{(1, 17)}$ = 1.315, p = 0.268, amplitude: $F_{(1, 17)}$ = 2.275, p = 0.151), however, spine density was significantly lower ($F_{(1, 16)}$ = 5.391, p = 0.035) in the *PV-Grik1*$^{-/-}$ as compared to controls (Figure 5D and E).

Maturation of PV+ neuron function regulates closure of the critical periods of plasticity and might thereby affect development of the glutamatergic connectivity. To study whether the loss of glutamatergic connectivity to principal neurons in *PV-Grik1*$^{-/-}$ mice was of developmental origin, we used our adult knockdown model. Interestingly, knockdown of GluK1 expression from PV+ neurons in the adult BLA (*PV-Grik1* KD) resulted in slightly higher frequency (p = 0.0399, Mann-Whitney) and amplitude (p = 0.0167, two tailed t-test) of sEPSCs in the BLA PNs as compared to controls (Figure 5C). Furthermore, the frequency of sIPSCs was higher in *PV-Grik1* KD slices (p = 0.0330, two tailed t test) while sIPSC amplitudes were unaltered between the two groups (Figure 5C). However, *PV-Grik1* KD slices, spine density in the principal neurons was not significantly different from controls ($F_{(1, 16)}$ = 0.153, p = 0.701, one-way ANOVA) (Figure 5E). Thus, acute and chronic (developmental) ablation of the GluK1 expression from PV+ neurons has distinct effects on synaptic transmission and glutamatergic connectivity to BLA principal neurons.

Together, our data suggests that impaired PV+ neuron function in the absence of GluK1 expression can be largely compensated for at the network level, to maintain the excitability and GABAergic drive of the BLA PN's. In contrast, we detected developmentally originating persistent alterations in glutamatergic synaptic transmission and connectivity.

Elimination of GluK1 in PV+ interneurons affects feedforward inhibition and synaptic plasticity in the BLA

PV+ interneurons are directly activated by cortical inputs, to mediate feedforward inhibition (FFI) in the BLA circuitry. In addition, PV+ neuron excitability gates activation of the somatostatin interneurons, which disinhibits the circuitry mediating dendritic FFI in the BLA (Englund et al., 2021; Wolff et al., 2014). Since PV+ neuron excitability was significantly perturbed in *PV-Grik1*$^{-/-}$ mice, we sought to understand if FFI, directed at BLA PNs was also altered. To this end, we did whole-cell voltage clamp recordings from BLA PNs and recorded the ratio of evoked excitatory and disynaptic inhibitory postsynaptic currents (EPSC/dIPSC ratio), in response to stimulation of the cortical inputs to BLA. We found that FFI is significantly stronger in *PV-Grik1*$^{-/-}$ mice as compared to controls ($F_{(1, 16)} = 5.144$, $p = 0.039$) (Figure 6A), suggesting that GluK1 ablation in the PV+ neurons predominantly affected the BLA disinhibitory microcircuit.

Since FFI is one of the key mechanisms controlling induction of synaptic plasticity in the BLA, we further wanted to study whether long-term potentiation (LTP) was disrupted in the *PV-Grik1*$^{-/-}$ mice. To this end, we performed extracellular field recordings from the lateral amygdala (LA) while stimulating the cortical afferents. Theta-burst stimulation (TBS) reliably induced a small but stabile synaptic potentiation in the control mice (Figure 6B). In contrast, in the *PV-Grik1*$^{-/-}$ mice, TBS resulted in short–term potentiation, after which the synaptic responses returned back to the basal level. The TBS induced changes in synaptic strength were significantly different between genotypes ($F_{(1, 15)} = 5.975$, $p = 0.028$) (Figure 6B).

Impaired LTP in the *PV-Grik1*$^{-/-}$ mice is consistent with lower glutamatergic drive and increased FFI directed at the LA principal neurons, both of which increase the threshold for activation of NMDA receptors.

Absence of GluK1 in PV+ interneurons results in hyperactivity and fear of novelty

Finally, we wanted to investigate the behavioral consequences ensuing from the loss of GluK1 in PV+ interneurons. We subjected littermate *Grik1*^{tm1c} and *PV-Grik1*$^{-/-}$ mice (heterozygous for *Cre*) to open-field (OF), elevated plus maze (EPM) and fear-conditioning (FC) behavioral assays. Interestingly, although both GluK1 and PV+ neurons have been implicated in anxiety (Ko et al.,

2015; Luo et al., 2020; Englund et al., 2021) the *PV-Grik1*$^{-/-}$ mice did not display a classical anxiety-like phenotype in the EPM or OF, as no significant differences between the genotypes were observed in the time spent in the open arm or center zone, respectively. However, the total distance travelled in the open field by *PV-Grik1*$^{-/-}$ mice was significantly higher than their littermate controls, suggesting a hyperactive phenotype ($F_{(1, 40)} = 5.461$, $p = 0.0245$, two-way ANOVA) (Figure 6C).

The FC paradigm revealed no impairments in contextual or cue-dependent fear learning. However, the *PV-Grik1*$^{-/-}$ mice displayed fear of novelty. % time spent freezing was not different between genotypes under basal conditions, but was significantly higher in *PV-Grik1*$^{-/-}$ mice as compared to the littermate controls in a novel context ($F_{(1, 36)} = 4.324$, $p = 0.0448$, 2-way ANOVA) and when presented with a novel tone ($F_{(1, 36)} = 11.88$, $p = 0.0015$, 2-way ANOVA) (Figure 6D). These behavioral results suggest crucial function of GluK1 in PV+ interneurons in brain circuits encoding novelty detection and fear, both of which are suggested to involve amygdala (Balderston et al., 2013)

Discussion

Kainate receptors are powerful regulators of GABAergic transmission in the adult brain (Akgül & McBain, 2016; Contractor et al., 2011). While strongly implicated in development of glutamatergic synapses and excitatory circuitry (Lauri et al., 2021), less information exists on the roles of KARs in the development and maturation of GABAergic interneurons (Segerstråle et al., 2010; Orav et al., 2019; Jack et al., 2019). Our present results indicate a pivotal role of GluK1 KARs in the specification of PV+ neuron phenotype during development and in maintaining the PV+ neuron specific features in the adult BLA.

Constituting the largest subpopulation of cortical interneurons (~40%) (Rudy et al., 2011), parvalbumin expressing (PV+) interneurons play crucial roles in encephalic functions. Interestingly, PV interneurons are also the most vulnerable population of interneurons (Marín, 2012; Nahar et al., 2021; Ruden et al., 2020) and their dysfunction is hence implicated in a multitude of neuropsychiatric and neurological disorders (Ferguson & Gao, 2018; Kaar et al., 2019; Marín, 2012). PV interneurons exert their crucial functions and are distinctive by their

unique properties such as high AP frequency, relatively low input resistance, and high-amplitude rapid after-hyperpolarization (Ascoli et al., 2008; Defelipe et al., 2013; Hu et al., 2014). These characteristic electrophysiological attributes were lost when GluK1 expression was eliminated, which may point to the etiological mechanisms of neurodevelopmental disorders where both KARs and PV+ neurons are implicated, including e.g. mood-and anxiety disorders and schizophrenia (Pickard et al. 2006; Powell et al. 2012; Lowry et al. 2013; Guadagno et al., 2021; Englund et al. 2021).

GluK1 expression regulates development and maintenance of the PV+ neuron phenotype

While NMDA-R mediated signaling has been identified to be critical for maturation of PV+ neurons (De Marco García et al. 2011, 2015; Belforte et al., 2010; Korotkova et al. 2010; Jeevakumar and Kroener 2016; Hanson et al., 2019; Mahadevan et al. 2021), no previous data on KARs in this context exists. Here, we confirm that GluK1 subunit containing KARs contribute to glutamatergic drive onto PV+ interneurons during postnatal development, before they are fully mature. In the absence of GluK1 signaling, PV+ neurons failed to acquire their adult phenotype and were characterized by low PV expression levels and low excitability throughout development. Furthermore, GluK1 lacking PV+ neurons failed to integrate into the surrounding glutamatergic network and received significantly less glutamatergic inputs (sEPSCs) in the adult stage as compared to controls. Interestingly, this phenotype was not observed in the juveniles, where the sEPSC frequency was slightly higher than in controls. We postulate that the elevated frequency of sEPSCs in juveniles reflects a developmentally restricted homeostatic compensatory mechanism to counter loss of GluK1 and consequent loss of PV cell excitability. However, other mechanisms such as developmental changes in the circuit excitability cannot be excluded.

Remarkably, loss of GluK1 function at adulthood was sufficient to induce significant PV+ cell dysfunction, involving loss of PV+ labeling, high frequency firing and glutamatergic input. Although these effects were not as robust as compared to *PV-Grik1*$^{-/-}$ mice, lacking GluK1 expression in the PV+ neurons throughout development, the finding suggests that GluK1 may regulate also the adult plasticity of PV+ neurons (Donato et al., 2013). Dynamic changes in PV+ neuron function in the adults has been implicated in cognitive processes such as memory encoding (Donato et al., 2013), but also in the context of stress (Woodward and Coutellier, 2021) and drug

actions (Winkel et al., 2021), however, the molecular mechanisms involved are not well understood.

The significant attenuation in PV+ cell excitability, coupled with the loss of electrophysiological signatures such as AP halfwidth and high amplitude AHP current point to aberrant expression or function of voltage gated Kv3 potassium channels in the absence of GluK1. Typically, PV+ cell maturation is accompanied by increased expression of Kv3 channels, which ensure fast action potential repolarization important for the high frequency firing (Chow et al., 1999; Hu et al., 2014, Du et al., 1996). The developmental reduction in AP-halfwidth was not observed in the GluK1 lacking PV+ neurons. In addition, high amplitude afterhyperpolarization, characteristic for PV+ neurons (Ascoli et al., 2008; DeFelipe et al., 2013; Hu et al., 2014), was also lost in the *PV-Grik1*$^{-/-}$ mice. Activation of GluK1 KARs can regulate voltage-gated channels via G-protein coupled signaling, which is implicated in regulation of neurotransmitter release and neuronal excitability (Lauri et al., 2006; Segerstrale et al., 2010; Pinheiro and Mulle 2008; Lerma and Marquez 2013). In particular, in immature hippocampal interneurons, G-protein coupled GluK1 KARs regulate the apamine-sensitive K+ currents responsible for the medium-duration afterhyperpolarization (mAHP), which directly influences the interneuron firing rate (Segerstrale et al., 2010). Our data suggest that the role of KARs in controlling voltage gated channels goes beyond these previously described, acute modulatory effects. The present results are consistent with a scenario where GluK1 signaling, likely via a G-protein coupled mechanism, is necessary to maintain the repertoire of voltage gated channels responsible for the unique membrane properties and specification of the PV+ neuron subtype.

Interestingly, both GluK1 and Kv3 channels are regulated by BDNF signaling via the TrkB receptors (Clarke et al., 2014; Sallert et al., 2009; Winkel et al., 2021), and the same signaling pathway is strongly implicated in both developmental maturation and adult plasticity of PV+ neurons (Gibel-Russo et al., 2022; Winkel et al., 2021).

Absence of GluK1 in the PV+ neurons causes broader amygdala dysfunction

Each PV+ interneuron makes multiple synaptic contacts to a vast number of principal neurons, so that even the perturbation of a single PV+ cell function could alter the surrounding network drastically (Powell et al. 2012). Surprisingly, despite the robust loss of PV+ neuron excitability, we detected no changes in the excitability or GABAergic input in the BLA principal neurons in

the *PV-Grik1*$^{-/-}$ mice. Apparently, the developmental aberrations in PV+ neuron function may be largely countered by compensatory changes in the network to maintain amygdala excitability.

PV interneurons also form strong connections with other interneurons, forming disinhibitory microcircuits that modulate feedforward inhibition (FFI) of principal neurons in the BLA (Wolf et al., 2014; Tremblay et al., 2016; Nahar et al., 2021). We have previously shown that the primary effect of GluK1 antagonism in the adult LA is an increase in FFI due to release of PV+ neuron mediated inhibitory control of somatostatin interneurons (Englund et al. 2021). Consistently, ablation of GluK1 in PV+ neurons resulted in an increase in the strength of FFI at cortical inputs to LA principal neurons, confirming that PV+ neuron GluK1 receptors are necessary for balancing FFI in the LA. Furthermore, consistent with the critical role of FFI in gating LTP induction (Bissiere et al., 2003; Haikonen et al., 2023), LTP in the cortical inputs to BLA was significantly attenuated in PV-*Grik1*$^{-/-}$ mice. Thus, while the some of the expected effects of PV+ neuron dysfunction on BLA circuit excitability appear to be developmentally compensated for, our data reveals an indispensable function for PV+ neuron GluK1 receptors in controlling the strength of FFI and consequently, threshold for LTP induction in the BLA.

Intriguingly, we also observed that glutamatergic drive to BLA neurons was clearly diminished in juvenile and significantly reduced in adult PV-*Grik1*$^{-/-}$ mice. This phenotype was of developmental origin, as it was not seen in response to knockdown of PV+ neuron GluK1 receptors in adults. Parallel changes in spine density further show that developmental ablation, but not adult knockdown of GluK1 expression in PV+ neurons results in lower glutamatergic connectivity to the BLA principal neurons. PV+ interneurons play a significant role in the development and fine tuning of cortical circuits and are vital for the closure of the critical period (Hensch, 2005). Since, in our model, PV+ interneurons don't seem to reach full maturity in the absence of GluK1, this could perturb the closure of the critical period. Prolonged critical period plasticity involving excessive synaptic pruning could explain the reduced glutamatergic drive on to BLA neurons we observe in our knockout model. Interestingly, precocious maturation of PV+ neurons during early life stress is thought to drive premature closure of the critical period plasticity and result in significant alterations in cortico-amygdaloid connectivity across development (Guadagno et al., 2018; Honeycutt et al., 2020; Manzano Nieves et al., 2020; Haikonen et al., 2023). We have gathered some preliminary evidence via functional ultrasound imaging that medial prefrontal

cortex (mPFC) to BLA resting state connectivity is impaired in PV-*Grik1*$^{-/-}$ mice. This supports that developmental dysfunction of GluK1 lacking PV+ interneurons may indeed disturb the activity-dependent refinement of the connectivity and result in persistent changes in the cortico-amygdaloid connectivity.

Behavioural outcomes of the PV+ neuron specific GluK1 ablation

Behavioral testing revealed that the PV-*Grik1*$^{-/-}$ mice were hyperactive and had increased fear of novelty. In contrast, ablation of GluK1 selectively in PV+ neurons was not sufficient to produce anxiety-like behavior, where these receptors have been previously implicated (Wu et al., 2017; Ryazantseva et al., 2020; Englund et al., 2021). However, both anxiety and fear of novelty depend on amygdala circuitry (eg Balderston et al., 2013), highlighting a role for GluK1 in regulating amygdala dependent behaviors.

KARs have been previously shown to regulate hyperactivity and psychomotor agitation (Lowry et al., 2013; Shaltiel et al., 2008; Xu et al., 2017). Our data extends these findings and suggests that this phenotype depends on KARs dysfunction in PV+ interneurons.

The existing research linking PV cell dysfunction to neuropsychiatric conditions, especially schizophrenia is extensive, comprising both of human and animal model studies (Harrington et al., 2016; Koh et al., 2016; Konradi et al., 2011; Lewis et al., 2012; Marín, 2012; Ruden et al., 2020). A majority of these studies reveal not only a diminishment in PV+ cell numbers and PV expression in several brain structures (Chung, Volk, et al., 2016; Powell et al. 2012; Volk et al., 2012; Wang et al., 2011), but also a loss of glutamatergic synapses in PV cells (Chung, Fish, et al., 2016). A similar loss of PV expression is seen in our knockout model and our results fall in line with existing literature on glutamatergic input to PV cells in the context of these disorders. Given these intricate and indubitable links, the results of our study may therefore be useful in interpreting and dissecting the etiological mechanisms in neuropsychiatric disorders such as schizophrenia.

In summary, we have shown the significance of GluK1 KARs in the functional and neurochemical maturation of PV+ interneurons in the BLA. The PV+ interneuron dysfunction in the absence of GluK1 associate with perturbations in BLA network function and behavior. These results illuminates the role of GluK1 KARs and PV cells in shaping BLA networks and provide scope for

designing effectual therapeutic methods for disorders that entail disrupted GluK1 and PV function.

Acknowledgements

We thank Janne Sulku, Vootele Voikar, the personnel in the Mouse Behavioural Phenotyping Facility and in the Laboratory Animal Center for expert technical help. This study was financially supported by the Academy of Finland, Sigrid Juselius Foundation, Magnus Ehrnrooth Foundation and Finnish Cultural Foundation. Mouse Behavioural Phenotyping Facility is supported by Biocenter Finland.

Author contributions

J.H. and R.S. carried out the vast majority of electrophysiological experiments and data analysis, and M.R and G.Z. contributed to these data. J.H, R.S and S.O performed the immunostainings and imaging. R.S and J.S performed the viral injections. The manuscript was written by J.H, R.S and S.E.L.

References

Akgül, G., & McBain, C. J. (2016). Diverse roles for ionotropic glutamate receptors on inhibitory interneurons in developing and adult brain. *The Journal of Physiology*, *594*(19), 5471–5490. https://doi.org/10.1113/JP271764

Anderson, W. W., & Collingridge, G. L. (2007). Capabilities of the WinLTP data acquisition program extending beyond basic LTP experimental functions. *Journal of Neuroscience Methods*, *162*(1–2), 346–356. https://doi.org/10.1016/j.jneumeth.2006.12.018

Balderston, N. L., Schultz, D. H., & Helmstetter, F. J. (2013). The Effect of Threat on Novelty Evoked Amygdala Responses. *PLoS ONE*, *8*(5), e63220. https://doi.org/10.1371/journal.pone.0063220

Belforte, J. E., Zsiros, V., Sklar, E. R., Jiang, Z., Yu, G., Li, Y., ... & Nakazawa, K. (2010). Postnatal NMDA receptor ablation in corticolimbic interneurons confers schizophrenia-like phenotypes. Nature neuroscience, 13(1), 76-83. https://doi.org/10.1038/nn.2447

Bissière, S., Humeau, Y., & Lüthi, A. (2003). Dopamine gates LTP induction in lateral amygdala by suppressing feedforward inhibition. Nature neuroscience, 6(6), 587-592. https://doi.org/10.1038/nn1058

Braga, M. F. M., Aroniadou-Anderjaska, V., Li, H., & Rogawski, M. A. (2009). Topiramate Reduces Excitability in the Basolateral Amygdala by Selectively Inhibiting GluK1 (GluR5) Kainate Receptors on Interneurons and Positively Modulating GABAA Receptors on Principal Neurons. *Journal of Pharmacology and Experimental Therapeutics*, *330*(2), 558–566. https://doi.org/10.1124/JPET.109.153908

Chow, A., Erisir, A., Farb, C., Nadal, M. S., Ozaita, A., Lau, D., Welker, E., & Rudy, B. (1999). K+ Channel Expression Distinguishes Subpopulations of Parvalbumin- and Somatostatin-Containing Neocortical Interneurons. *The Journal of Neuroscience*, *19*(21), 9332. https://doi.org/10.1523/JNEUROSCI.19-21-09332.1999

Clarke, V. R. J., Molchanova, S. M., Hirvonen, T., Taira, T., & Lauri, S. E. (2014). Activity-Dependent Upregulation of Presynaptic Kainate Receptors at Immature CA3–CA1 Synapses. *The Journal of Neuroscience*, *34*(50), 16902–16916. https://doi.org/10.1523/JNEUROSCI.1842-14.2014

Contractor, A., Mulle, C., & Swanson, G. T. (2011). Kainate receptors coming of age: Milestones of two decades of research. In *Trends in Neurosciences* (Vol. 34, Issue 3, pp. 154–163). https://doi.org/10.1016/j.tins.2010.12.002

Cossart, R., Esclapez, M., Hirsch, J. C., Bernard, C., & Ben-Ari, Y. (1998). GluR5 kainate receptor activation in interneurons increases tonic inhibition of pyramidal cells. *Nature Neuroscience*, *1*(6), 470–478. https://doi.org/10.1038/2185

De Marco García, N. V., Karayannis, T., & Fishell, G. (2011). Neuronal activity is required for the development of specific cortical interneuron subtypes. *Nature*, *472*(7343), 351–355. https://doi.org/10.1038/nature09865

De Marco García, N. V, Priya, R., Tuncdemir, S. N., Fishell, G., & Karayannis, T. (2015). Sensory inputs control the integration of neurogliaform interneurons into cortical circuits. *Nature Neuroscience*, *18*(3), 393–401. https://doi.org/10.1038/nn.3946

DeFelipe, J., López-Cruz, P. L., Benavides-Piccione, R., Bielza, C., Larrañaga, P., Anderson, S., Burkhalter, A., Cauli, B., Fairén, A., Feldmeyer, D., Fishell, G., Fitzpatrick, D., Freund, T. F., González-Burgos, G., Hestrin, S., Hill, S., Hof, P. R., Huang, J., Jones, E. G., … Ascoli, G. A. (2013). New insights into the classification and nomenclature of cortical GABAergic interneurons. *Nature Reviews Neuroscience*, *14*(3), 202–216. https://doi.org/10.1038/nrn3444

Dehorter, N., Ciceri, G., Bartolini, G., Lim, L., del Pino, I., & Marín, O. (2015). Tuning of fast-spiking interneuron properties by an activity-dependent transcriptional switch. *Science*, *349*(6253), 1216–1220. https://doi.org/10.1126/science.aab3415

Doischer, D., Aurel Hosp, J., Yanagawa, Y., Obata, K., Jonas, P., Vida, I., & Bartos, M. (2008). Postnatal Differentiation of Basket Cells from Slow to Fast Signaling Devices. *The Journal of Neuroscience*, *28*(48), 12956–12968. https://doi.org/10.1523/JNEUROSCI.2890-08.2008

Donato, F., Rompani, S. B., & Caroni, P. (2013). Parvalbumin-expressing basket-cell network plasticity induced by experience regulates adult learning. Nature, 504(7479), 272-276. https://doi.org/10.1038/nature12866

Du, J., Zhang, L., Weiser, M., Rudy, B., & McBain, C. J. (1996). Developmental expression and functional characterization of the potassium-channel subunit Kv3.1b in parvalbumin-containing interneurons

of the rat hippocampus. *The Journal of Neuroscience*, *16*(2), 506. https://doi.org/10.1523/JNEUROSCI.16-02-00506.1996

Englund, J., Haikonen, J., Shteinikov, V., Amarilla, S. P., Atanasova, T., Shintyapina, A., Ryazantseva, M., Partanen, J., Voikar, V., & Lauri, S. E. (2021). Downregulation of kainate receptors regulating GABAergic transmission in amygdala after early life stress is associated with anxiety-like behavior in rodents. *Translational Psychiatry*, *11*(1), 538. https://doi.org/10.1038/s41398-021-01654-7

Faber, E. S. L., Callister, R. J., & Sah, P. (2001). Morphological and electrophysiological properties of principal neurons in the rat lateral amygdala in vitro. *Journal of Neurophysiology*, *85*(2), 714–723. https://doi.org/10.1152/JN.2001.85.2.714/ASSET/IMAGES/LARGE/9K0211513010.JPEG

Ferguson, B. R., & Gao, W.-J. (2018). PV Interneurons: Critical Regulators of E/I Balance for Prefrontal Cortex-Dependent Behavior and Psychiatric Disorders. *Frontiers in Neural Circuits*, *12*. https://doi.org/10.3389/fncir.2018.00037

Gibel-Russo, R., Benacom, D., & Di Nardo, A. A. (2022). Non-Cell-Autonomous Factors Implicated in Parvalbumin Interneuron Maturation and Critical Periods. *Frontiers in Neural Circuits*, *16*. https://doi.org/10.3389/fncir.2022.875873

Goldberg, E. M., Jeong, H.-Y., Kruglikov, I., Tremblay, R., Lazarenko, R. M., & Rudy, B. (2011). Rapid Developmental Maturation of Neocortical FS Cell Intrinsic Excitability. *Cerebral Cortex*, *21*(3), 666–682. https://doi.org/10.1093/cercor/bhq138

Guadagno, A., Kang, M. S., Devenyi, G. A., Mathieu, A. P., Rosa-Neto, P., Chakravarty, M., & Walker, C. D. (2018). Reduced resting-state functional connectivity of the basolateral amygdala to the medial prefrontal cortex in preweaning rats exposed to chronic early-life stress. Brain Structure and Function, 223, 3711-3729. https://doi.org/10.1007/s00429-018-1720-3

Guadagno, A., Belliveau, C., Mechawar, N., & Walker, C.-D. (2021). Effects of Early Life Stress on the Developing Basolateral Amygdala-Prefrontal Cortex Circuit: The Emerging Role of Local Inhibition and Perineuronal Nets. *Frontiers in Human Neuroscience*, *15*. https://doi.org/10.3389/fnhum.2021.669120

Haikonen, J., Englund, J., Amarilla, S. P., Kharybina, Z., Shintyapina, A., Kegler, K., ... & Lauri, S. E. (2023). Aberrant cortical projections to amygdala GABAergic neurons contribute to developmental circuit dysfunction following early life stress. Iscience, 26(1). https://doi.org/10.1016/j.isci.2022.105724

Hanson, E., Armbruster, M., Lau, L. A., Sommer, M. E., Klaft, Z. J., Swanger, S. A., ... & Dulla, C. G. (2019). Tonic activation of GluN2C/GluN2D-containing NMDA receptors by ambient glutamate facilitates cortical interneuron maturation. Journal of Neuroscience, 39(19), 3611-3626. https://doi.org/10.1523/JNEUROSCI.1392-18.2019

Hensch, T. K. (2005). Critical period plasticity in local cortical circuits. *Nature Reviews Neuroscience*, *6*(11), 877–888. https://doi.org/10.1038/nrn1787

Honeycutt, J. A., Demaestri, C., Peterzell, S., Silveri, M. M., Cai, X., Kulkarni, P., ... & Brenhouse, H. C. (2020). Altered corticolimbic connectivity reveals sex-specific adolescent outcomes in a rat model of early life adversity. Elife, 9, e52651. https://doi.org/10.7554/eLife.52651

Hu, H., Gan, J., & Jonas, P. (2014). Fast-spiking, parvalbumin $^{+}$ GABAergic interneurons: From cellular design to microcircuit function. *Science*, *345*(6196). https://doi.org/10.1126/science.1255263

Jack, A., Hamad, M. I. K., Gonda, S., Gralla, S., Pahl, S., Hollmann, M., & Wahle, P. (2019). Development of Cortical Pyramidal Cell and Interneuronal Dendrites: a Role for Kainate Receptor Subunits and NETO1. *Molecular Neurobiology*, *56*(7), 4960–4979. https://doi.org/10.1007/s12035-018-1414-0

Jane, D. E., Lodge, D., & Collingridge, G. L. (2009). Kainate receptors: pharmacology, function and therapeutic potential. Neuropharmacology, 56(1), 90-113. https://doi.org/10.1016/j.neuropharm.2008.08.023

Jeevakumar, V., & Kroener, S. (2016). Ketamine administration during the second postnatal week alters synaptic properties of fast-spiking interneurons in the medial prefrontal cortex of adult mice. Cerebral cortex, 26(3), 1117-1129. https://doi.org/10.1093/cercor/bhu293

Kaar, S. J., Angelescu, I., Marques, T. R., & Howes, O. D. (2019). Pre-frontal parvalbumin interneurons in schizophrenia: a meta-analysis of post-mortem studies. *Journal of Neural Transmission*, *126*(12), 1637–1651. https://doi.org/10.1007/s00702-019-02080-2

Korotkova, T., Fuchs, E. C., Ponomarenko, A., von Engelhardt, J., & Monyer, H. (2010). NMDA Receptor Ablation on Parvalbumin-Positive Interneurons Impairs Hippocampal Synchrony, Spatial Representations, and Working Memory. *Neuron*, *68*(3), 557–569. https://doi.org/10.1016/j.neuron.2010.09.017

Lanore, F., Labrousse, V. F., Szabo, Z., Normand, E., Blanchet, C., & Mulle, C. (2012). Deficits in Morphofunctional Maturation of Hippocampal Mossy Fiber Synapses in a Mouse Model of Intellectual Disability. *The Journal of Neuroscience*, *32*(49), 17882–17893. https://doi.org/10.1523/JNEUROSCI.2049-12.2012

Lauri, S. E., Ryazantseva, M., Orav, E., Vesikansa, A., & Taira, T. (2021). Kainate receptors in the developing neuronal networks. *Neuropharmacology*, *195*, 108585. https://doi.org/10.1016/J.NEUROPHARM.2021.108585

Lauri, S. E., Segerstråle, M., Vesikansa, A., Maingret, F., Mulle, C., Collingridge, G. L., Isaac, J. T. R., & Taira, T. (2005). Endogenous Activation of Kainate Receptors Regulates Glutamate Release and Network Activity in the Developing Hippocampus. *The Journal of Neuroscience*, *25*(18), 4473–4484. https://doi.org/10.1523/JNEUROSCI.4050-04.2005

Lauri, S. E., Vesikansa, A., Segerstråle, M., Collingridge, G. L., Isaac, J. T. R., & Taira, T. (2006). Functional Maturation of CA1 Synapses Involves Activity-Dependent Loss of Tonic Kainate Receptor-Mediated Inhibition of Glutamate Release. *Neuron*, *50*(3), 415–429. https://doi.org/10.1016/j.neuron.2006.03.020

Lerma, J., & Marques, J. M. (2013). Kainate receptors in health and disease. In *Neuron* (Vol. 80, Issue 2, pp. 292–311). https://doi.org/10.1016/j.neuron.2013.09.045

Lowry, E. R., Kruyer, A., Norris, E. H., Cederroth, C. R., & Strickland, S. (2013). The GluK4 kainate receptor subunit regulates memory, mood, and excitotoxic neurodegeneration. *Neuroscience*, *235*, 215–225. https://doi.org/10.1016/j.neuroscience.2013.01.029

Luo, Z.-Y., Huang, L., Lin, S., Yin, Y.-N., Jie, W., Hu, N.-Y., Hu, Y.-Y., Guan, Y.-F., Liu, J.-H., You, Q.-L., Chen, Y.-H., Luo, Z.-C., Zhang, S.-R., Li, X.-W., Yang, J.-M., Tao, Y.-M., Mei, L., & Gao, T.-M. (2020). Erbin in Amygdala Parvalbumin-Positive Neurons Modulates Anxiety-like Behaviors. *Biological Psychiatry*, *87*(10), 926–936. https://doi.org/10.1016/j.biopsych.2019.10.021

Mahadevan, V., Mitra, A., Zhang, Y., Yuan, X., Peltekian, A., Chittajallu, R., Esnault, C., Maric, D., Rhodes, C., Pelkey, K. A., Dale, R., Petros, T. J., & McBain, C. J. (2021). NMDARs Drive the Expression of Neuropsychiatric Disorder Risk Genes Within GABAergic Interneuron Subtypes in the Juvenile Brain. *Frontiers in Molecular Neuroscience*, *14*. https://doi.org/10.3389/fnmol.2021.712609

Mahanty, N. K., & Sah, P. (1998). Calcium-permeable AMPA receptors mediate long-term potentiation in interneurons in the amygdala. *Nature*, *394*(6694), 683–687. https://doi.org/10.1038/29312

Manzano Nieves, G., Bravo, M., Baskoylu, S., & Bath, K. G. (2020). Early life adversity decreases pre-adolescent fear expression by accelerating amygdala PV cell development. Elife, 9, e55263. https://doi.org/10.7554/eLife.55263

Marín, O. (2012). Interneuron dysfunction in psychiatric disorders. *Nature Reviews Neuroscience*, *13*(2), 107–120. https://doi.org/10.1038/nrn3155

Marques, J. M., Rodrigues, R. J., Valbuena, S., Rozas, J. L., Selak, S., Marin, P., Aller, M. I., & Lerma, J. (2013). CRMP2 Tethers Kainate Receptor Activity to Cytoskeleton Dynamics during Neuronal Maturation. *The Journal of Neuroscience*, *33*(46), 18298–18310. https://doi.org/10.1523/JNEUROSCI.3136-13.2013

Mulle, C., & Crépel, V. (2021). Regulation and dysregulation of neuronal circuits by KARs. Neuropharmacology, 197, 108699. https://doi.org/10.1016/j.neuropharm.2021.108699

Nahar, L., Delacroix, B. M., & Nam, H. W. (2021). The Role of Parvalbumin Interneurons in Neurotransmitter Balance and Neurological Disease. *Frontiers in Psychiatry*, *12*. https://doi.org/10.3389/fpsyt.2021.679960

Nair, J. D., Wilkinson, K. A., Henley, J. M., & Mellor, J. R. (2021). Kainate receptors and synaptic plasticity. *Neuropharmacology*, *196*, 108540. https://doi.org/10.1016/j.neuropharm.2021.108540

Ojanen, S., Kuznetsova, T., Kharybina, Z., Voikar, V., Lauri, S. E., & Taira, T. (2023). Interneuronal GluK1 kainate receptors control maturation of GABAergic transmission and network synchrony in the hippocampus. *Molecular Brain*, *16*(1), 43. https://doi.org/10.1186/s13041-023-01035-9

Orav, E., Atanasova, T., Shintyapina, A., Kesaf, S., Kokko, M., Partanen, J., Taira, T., & Lauri, S. E. (2017). NETO1 Guides Development of Glutamatergic Connectivity in the Hippocampus by Regulating Axonal Kainate Receptors. *Eneuro*, *4*(3), ENEURO.0048-17.2017. https://doi.org/10.1523/ENEURO.0048-17.2017

Pafundo, D. E., Pretell Annan, C. A., Fulginiti, N. M., & Belforte, J. E. (2021). Early NMDA Receptor Ablation in Interneurons Causes an Activity-Dependent E/I Imbalance in vivo in Prefrontal Cortex Pyramidal

Neurons of a Mouse Model Useful for the Study of Schizophrenia. *Schizophrenia Bulletin*, *47*(5), 1300–1309. https://doi.org/10.1093/schbul/sbab030

Petrovic, M. M., Viana da Silva, S., Clement, J. P., Vyklicky, L., Mulle, C., González-González, I. M., & Henley, J. M. (2017). Metabotropic action of postsynaptic kainate receptors triggers hippocampal long-term potentiation. *Nature Neuroscience*, *20*(4), 529–539. https://doi.org/10.1038/nn.4505

Pickard, B. S., Malloy, M. P., Christoforou, A., Thomson, P. A., Evans, K. L., Morris, S. W., ... & Muir, W. J. (2006). Cytogenetic and genetic evidence supports a role for the kainate-type glutamate receptor gene, GRIK4, in schizophrenia and bipolar disorder. Molecular psychiatry, 11(9), 847-857. https://doi.org/10.1038/sj.mp.4001867

Pinheiro, P., & Mulle, C. (2006). Kainate receptors. *Cell and Tissue Research*, *326*(2), 457–482. https://doi.org/10.1007/s00441-006-0265-6

Powell, S. B., Sejnowski, T. J., & Behrens, M. M. (2012). Behavioral and neurochemical consequences of cortical oxidative stress on parvalbumin-interneuron maturation in rodent models of schizophrenia. Neuropharmacology, 62(3), 1322-1331. https://doi.org/10.1016/j.neuropharm.2011.01.049

Rainnie, D. G., Mania, I., Mascagni, F., & McDonald, A. J. (2006). Physiological and morphological characterization of parvalbumin-containing interneurons of the rat basolateral amygdala. *Journal of Comparative Neurology*, *498*(1), 142–161. https://doi.org/10.1002/CNE.21049

Ruden, J. B., Dugan, L. L., & Konradi, C. (2021). Parvalbumin interneuron vulnerability and brain disorders. *Neuropsychopharmacology*, *46*(2), 279–287. https://doi.org/10.1038/s41386-020-0778-9

Rudy, B., Fishell, G., Lee, S., & Hjerling-Leffler, J. (2011). Three groups of interneurons account for nearly 100% of neocortical GABAergic neurons. *Developmental Neurobiology*, *71*(1), 45–61. https://doi.org/10.1002/dneu.20853

Ryazantseva, M., Englund, J., Shintyapina, A., Huupponen, J., Shteinikov, V., Pitkänen, A., Partanen, J. M., & Lauri, S. E. (2020). Kainate receptors regulate development of glutamatergic synaptic circuitry in the rodent amygdala. *ELife*, *9*. https://doi.org/10.7554/eLife.52798

Sakha, P., Vesikansa, A., Orav, E., Heikkinen, J., Kukko-Lukjanov, T.-K., Shintyapina, A., Franssila, S., Jokinen, V., Huttunen, H. J., & Lauri, S. E. (2016). Axonal Kainate Receptors Modulate the Strength of

Efferent Connectivity by Regulating Presynaptic Differentiation. *Frontiers in Cellular Neuroscience*, *10*. https://doi.org/10.3389/fncel.2016.00003

Sallert, M., Rantamäki, T., Vesikansa, A., Anthoni, H., Harju, K., Yli-Kauhaluoma, J., Taira, T., Castren, E., & Lauri, S. E. (2009a). Brain-Derived Neurotrophic Factor Controls Activity-Dependent Maturation of CA1 Synapses by Downregulating Tonic Activationof Presynaptic Kainate Receptors. *Journal of Neuroscience*, *29*(36), 11294–11303. https://doi.org/10.1523/JNEUROSCI.0560-09.2009

Sallert, M., Rantamäki, T., Vesikansa, A., Anthoni, H., Harju, K., Yli-Kauhaluoma, J., Taira, T., Castren, E., & Lauri, S. E. (2009b). Brain-Derived Neurotrophic Factor Controls Activity-Dependent Maturation of CA1 Synapses by Downregulating Tonic Activationof Presynaptic Kainate Receptors. *Journal of Neuroscience*, *29*(36), 11294–11303. https://doi.org/10.1523/JNEUROSCI.0560-09.2009

Segerstråle, M., Juuri, J., Lanore, F., Piepponen, P., Lauri, S. E., Mulle, C., & Taira, T. (2010). High firing rate of neonatal hippocampal interneurons is caused by attenuation of afterhyperpolarizing potassium currents by tonically active kainate receptors. Journal of Neuroscience, 30(19), 6507-6514. https://doi.org/10.1523/JNEUROSCI.4856-09.2010

Semyanov, A., & Kullmann, D. M. (2001). Kainate receptor-dependent axonal depolarization and action potential initiation in interneurons. *Nature Neuroscience*, *4*(7), 718–723. https://doi.org/10.1038/89506

Shaltiel, G., Maeng, S., Malkesman, O., Pearson, B., Schloesser, R. J., Tragon, T., Rogawski, M., Gasior, M., Luckenbaugh, D., Chen, G., & Manji, H. K. (2008). Evidence for the involvement of the kainate receptor subunit GluR6 (GRIK2) in mediating behavioral displays related to behavioral symptoms of mania. *Molecular Psychiatry*, *13*(9), 858–872. https://doi.org/10.1038/mp.2008.20

Tashiro, A., Dunaevsky, A., Blazeski, R., Mason, C. A., & Yuste, R. (2003). Bidirectional Regulation of Hippocampal Mossy Fiber Filopodial Motility by Kainate Receptors. *Neuron*, *38*(5), 773–784. https://doi.org/10.1016/S0896-6273(03)00299-X

Tremblay, R., Lee, S., & Rudy, B. (2016). GABAergic Interneurons in the Neocortex: From Cellular Properties to Circuits. *Neuron*, *91*(2), 260–292. https://doi.org/10.1016/j.neuron.2016.06.033

Valbuena, S., & Lerma, J. (2021). Losing balance: Kainate receptors and psychiatric disorders comorbidities. Neuropharmacology, 191, 108558. https://doi.org/10.1016/j.neuropharm.2021.108558

Vesikansa, A., Sakha, P., Kuja-Panula, J., Molchanova, S., Rivera, C., Huttunen, H. J., Rauvala, H., Taira, T., & Lauri, S. E. (2012). Expression of GluK1c underlies the developmental switch in presynaptic kainate receptor function. *Scientific Reports*, *2*(1), 310. https://doi.org/10.1038/srep00310

Wamsley, B., & Fishell, G. (2017). Genetic and activity-dependent mechanisms underlying interneuron diversity. *Nature Reviews Neuroscience*, *18*(5), 299–309. https://doi.org/10.1038/nrn.2017.30

Winkel, F., Ryazantseva, M., Voigt, M. B., Didio, G., Lilja, A., Llach Pou, M., Steinzeig, A., Harkki, J., Englund, J., Khirug, S., Rivera, C., Palva, S., Taira, T., Lauri, S. E., Umemori, J., & Castrén, E. (2021). Pharmacological and optical activation of TrkB in Parvalbumin interneurons regulate intrinsic states to orchestrate cortical plasticity. *Molecular Psychiatry*, *26*(12), 7247. https://doi.org/10.1038/S41380-021-01211-0

Wolff, S. B. E., Gründemann, J., Tovote, P., Krabbe, S., Jacobson, G. A., Müller, C., Herry, C., Ehrlich, I., Friedrich, R. W., Letzkus, J. J., & Lüthi, A. (2014). Amygdala interneuron subtypes control fear learning through disinhibition. *Nature*, *509*(7501), 453–458. https://doi.org/10.1038/nature13258

Woodward, E. M., & Coutellier, L. (2021). Age-and sex-specific effects of stress on parvalbumin interneurons in preclinical models: Relevance to sex differences in clinical neuropsychiatric and neurodevelopmental disorders. Neuroscience & Biobehavioral Reviews, 131, 1228-1242. https://doi.org/10.1016/j.neubiorev.2021.10.031

Wyeth, M. S., Pelkey, K. A., Yuan, X., Vargish, G., Johnston, A. D., Hunt, S., Fang, C., Abebe, D., Mahadevan, V., Fisahn, A., Salter, M. W., McInnes, R. R., Chittajallu, R., & McBain, C. J. (2017). Neto Auxiliary Subunits Regulate Interneuron Somatodendritic and Presynaptic Kainate Receptors to Control Network Inhibition. *Cell Reports*, *20*(9), 2156–2168. https://doi.org/10.1016/j.celrep.2017.08.017

Xu, J., Marshall, J. J., Fernandes, H. B., Nomura, T., Copits, B. A., Procissi, D., ... & Contractor, A. (2017). Complete disruption of the kainate receptor gene family results in corticostriatal dysfunction in mice. Cell reports, 18(8), 1848-1857. http://dx.doi.org/10.1016/j.celrep.2017.01.073

FIGURE 1

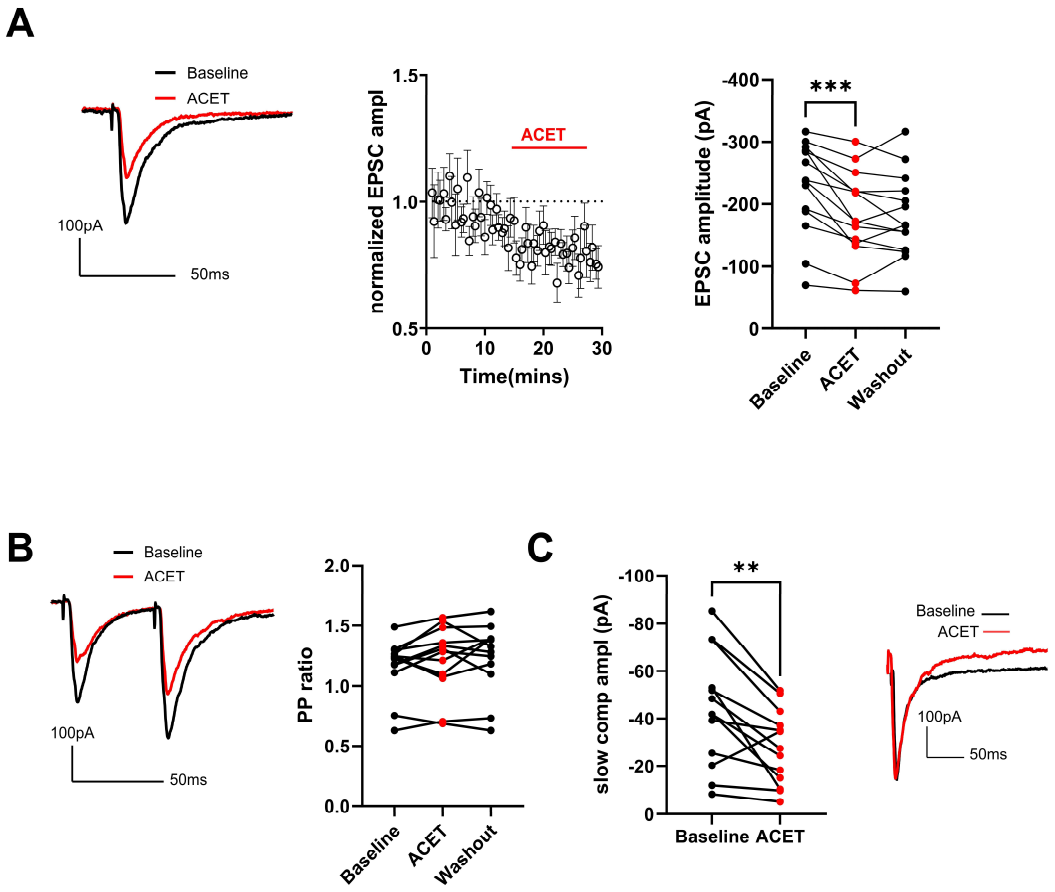

Figure 1. GluK1 subunit containing KARs regulate glutamatergic synaptic transmission at the cortical inputs to BLA PV+ interneurons in the juvenile BLA. **A.** Example traces and quantification of evoked excitatory post synaptic current (EPSC) amplitudes from PV+ cells of 16-18 day old PV-Tdtomato mice, before and after 200 nM ACET application (right) (n = 14 cells, 4 animals) ***$p < 0.001$, paired t-test. **B**. Example traces and quantification of paired pulse (PP) ratio of EPSCs before and after ACET application, from the same cells as in A. **C**. Quantification of the effects of ACET on the amplitude of slow component of the EPSC in PV+ neurons. Example traces represent scaled and superimposed EPSC before and during ACET application. *$p = 0.002$, paired t-test**.**

FIGURE 2

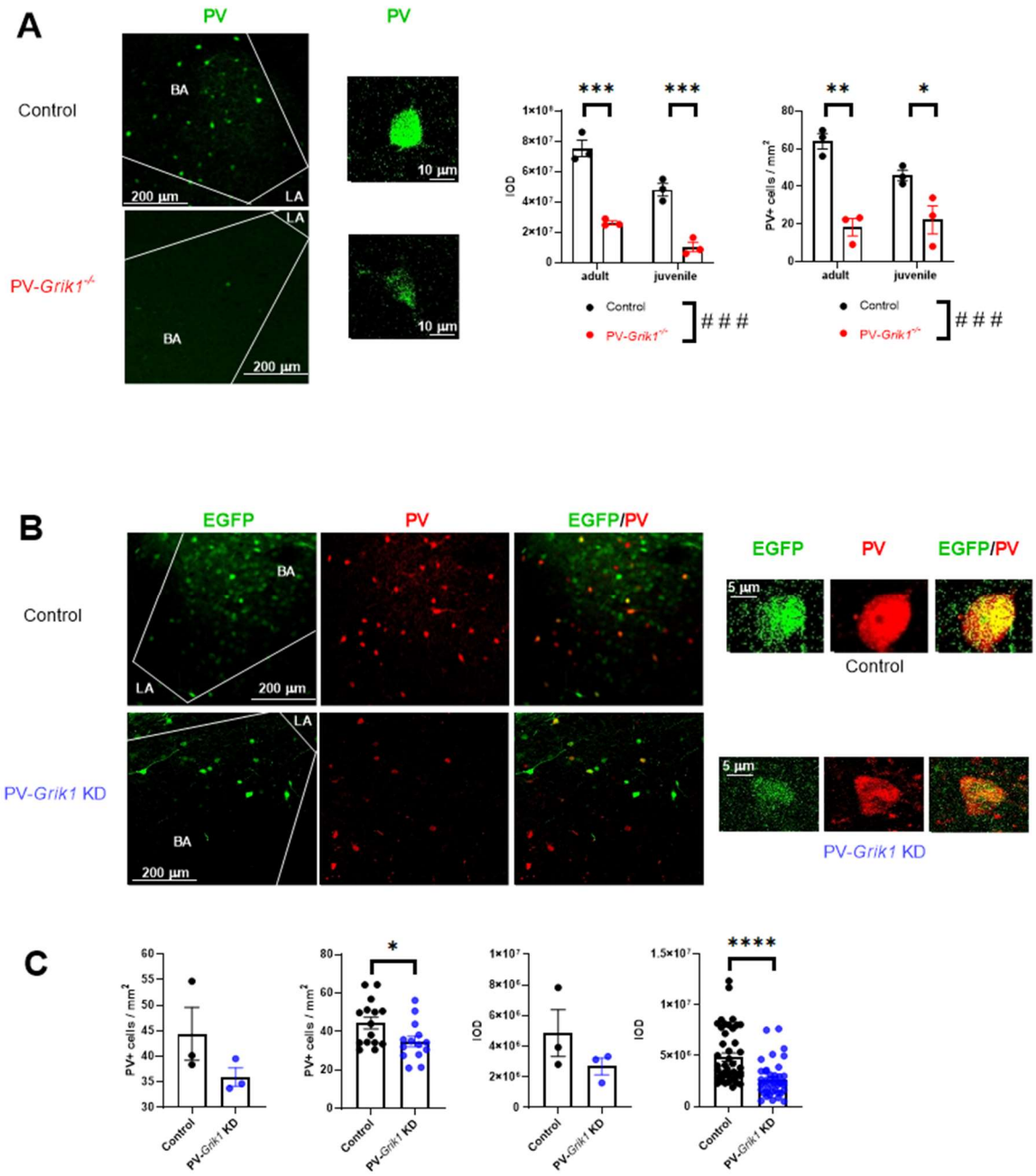

Figure 2. GluK1 lacking PV+ interneurons are characterized by low PV expression. **A.** Example pictures of PV (green) immunostaining in the BLA of adult control (top row) and *PV-Grik1*$^{-/-}$ (bottom row) mice and enlarged images of a single control (top) and *PV-Grik1*$^{-/-}$ (bottom) PV+ neuron. On the right, quantification of the IOD and PV+ cell densities in both adult and juvenile BLA. The data consists of 3 animals per group and 5 - 8 slices per animal. *p < 0.05; ***p < 0.001; Holm-Sidak, ### p < 0.001; 2-way ANOVA. **B.** Example pictures of PV (red) immunostainings in the BLA of adult *Grik1*^{tm1c} mice, transduced with AAV viruses encoding for PV-EGFP (green; top row; control), or PV-CRE-EGFP (green, bottom row; *PV-Grik1* KD). On the right, enlarged example pictures of single EGFP expressing PV+ cells in both groups. **C.** Quantification of PV+ cell density and IOD from control and *PV-Grik1* KD adult mice. The data consists of 3 animals per group and 5-8 slices per animal. *p < 0.05; ***p < 0.001; one-way repeated measures ANOVA.

FIGURE 3

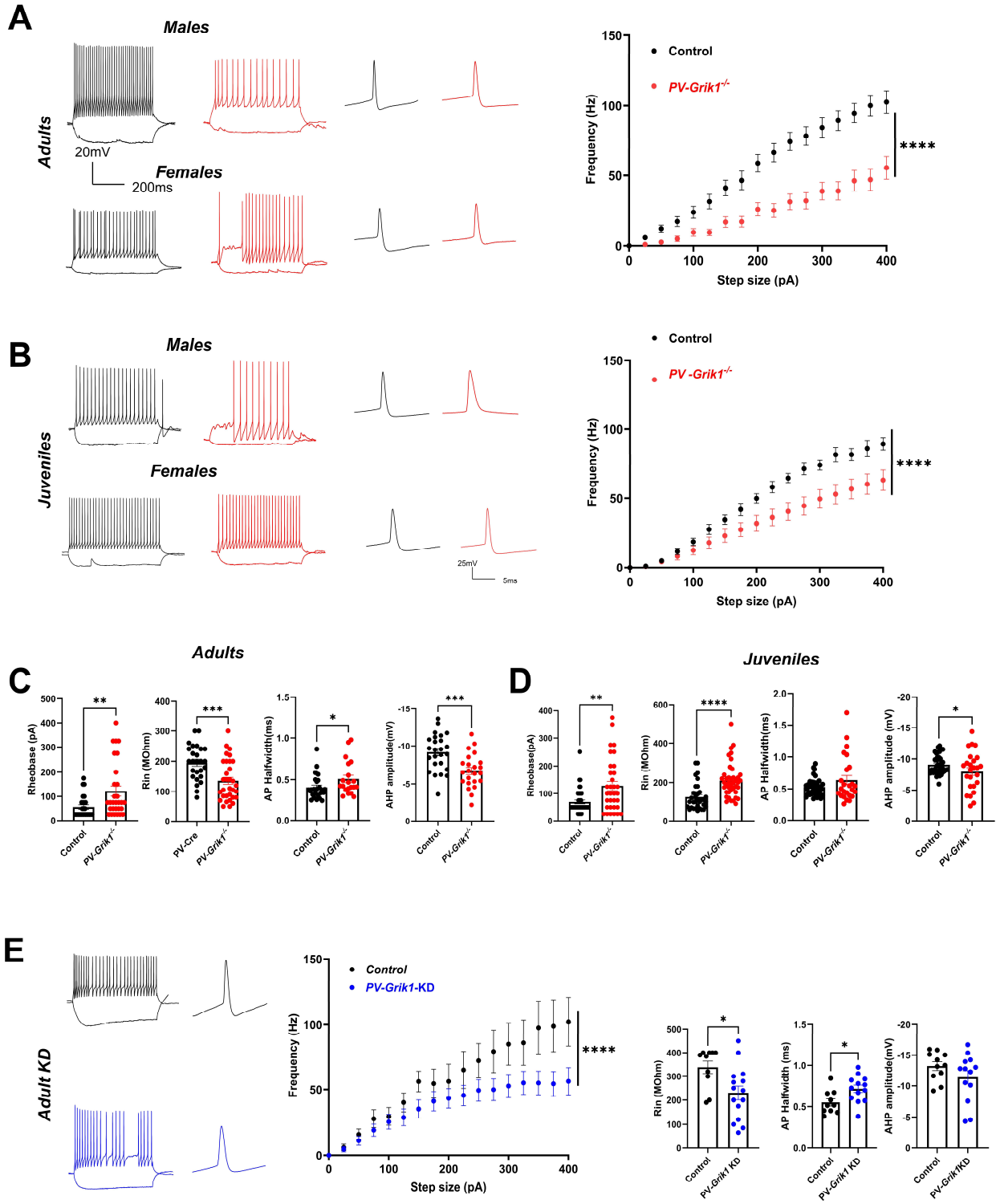

Figure 3. Absence of GluK1 results in low PV+ cell excitability across and beyond development. **A.** Example traces illustrating PV+ cell response to depolarizing step (200 pA) and action potential kinetics (middle) from adult control (*PV-Cre,* black traces) and *PV-Grik1*$^{-/-}$ (red traces) mice. Quantification of the firing frequency of PV+ neurons in response to depolarizing current steps (right) (control: n = 25 cells, 8 animals, *PV-Grik1*$^{-/-}$: n = 29 cells, 7 animals) ****p < 0.0001, Mixed effects model (REML). **B.** Similar data from juvenile mice (control: n = 41 cells, 8 animals, *PV-Grik1*$^{-}$

$^{-/-}$: n = 34 cells, 8 animals) ****p < 0.0001, Mixed effects model (REML). **C.** Quantification of rheobase, input resistance, AP half-width and after-hyperpolarization (AHP) current amplitudes of PV+ cells of adult control and *PV-Grik1*$^{-/-}$ mice. *p < 0.05; **p < 0.01; ***p < 0.001, Mann-Whitney. **D.** Similar data as in C, from juvenile mice. *p < 0.05; **p < 0.01; ***p < 0.001, ****p < 0.0001, Mann-Whitney. **E.** Example traces of PV+ cell excitability (left), action potential kinetics (left), as well as quantification of PV+ cell excitability data (middle) from adult male control (black traces) and PV-*Grik1* KD mice (blue traces) (control: n = 10 cells, 3 animals, PV-*Grik1* KD*:* n = 15 cells, 3 animals) ****p < 0.0001, Mixed effects model (REML). On the right, quantification of the passive and active membrane properties for the same cells. *p < 0.05; Mann-Whitney.

FIGURE 4

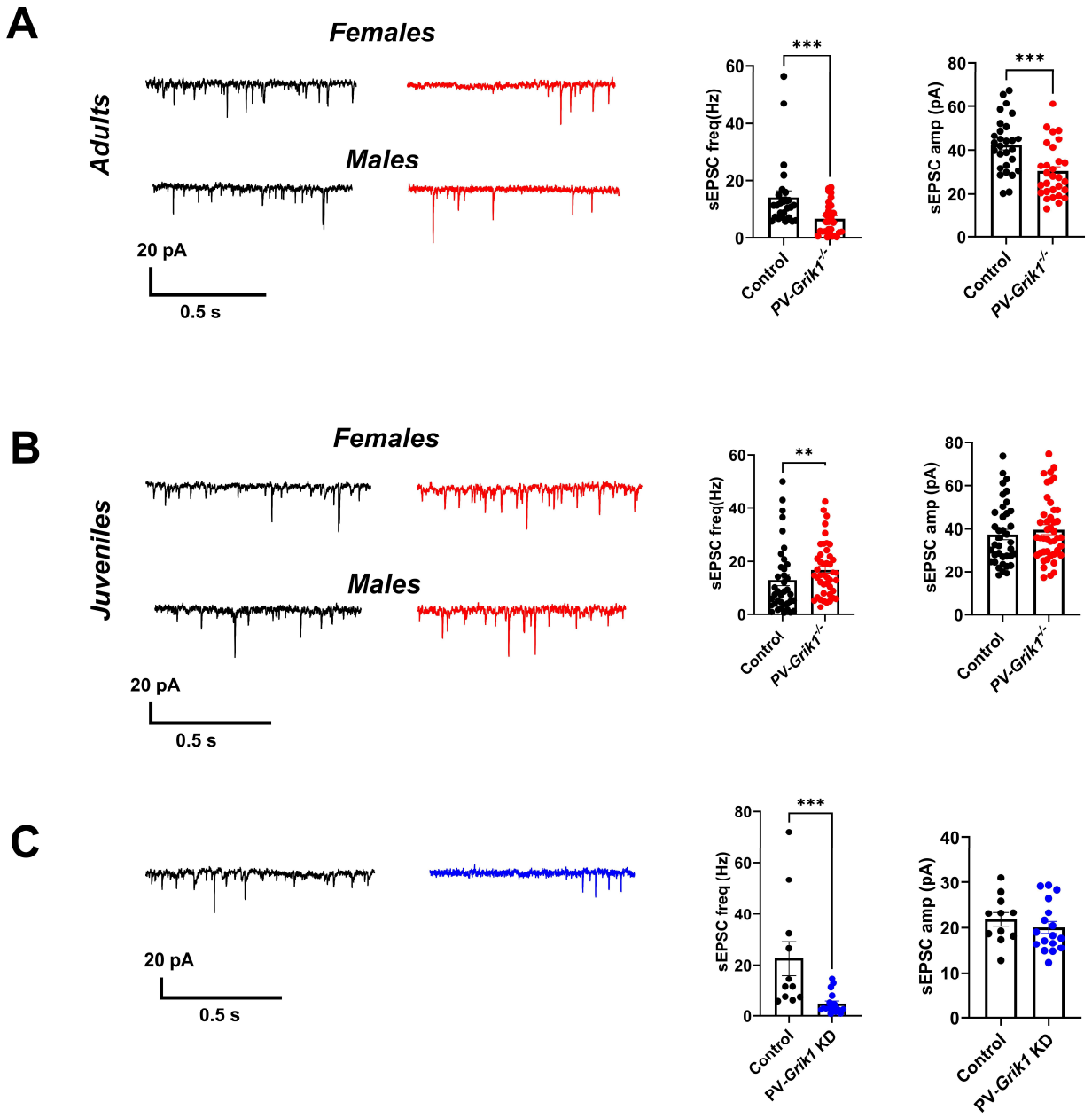

Figure 4. Absence of GluK1 perturbs glutamatergic input to PV+ cells across and beyond development. **A.** Example traces (left) and quantification (right) of PV+ cell sEPSC frequency (males and females pooled) and amplitude in adult control (*PV-Cre,* black traces) and knockout (*PV-Grik1*$^{-/-}$, red traces) mice (control: n = 28 cells, 8 animals *PV-Grik1*$^{-/-}$: n = 29 cells, 7 animals) ***p < 0.001; **** p < 0.0001, Mann-Whitney. **B.** Example traces (left; control: black traces, *PV-Grik1*$^{-/-}$*:* red traces) and quantification (right) of PV+ cell sEPSC frequency and amplitude in juvenile (males and females pooled) control (n = 38 cells, 9 animals) and *PV-Grik1*$^{-/-}$ (n = 34 cells, 10 animals) mice **p < 0.01, Mann-Whitney. **C.** Example traces (left) and quantification (right) of PV+ cell sEPSC frequency and amplitude in male adult control (PV-Cre, black trace) and viral knockdown (PV-*Grik1* KD, blue trace) mice (control: n = 11 cells, 3 animals, PV-*Grik1* KD*:* n = 17 cells, 3 animals) ***p < 0.001; Mann-Whitney.

FIGURE 5

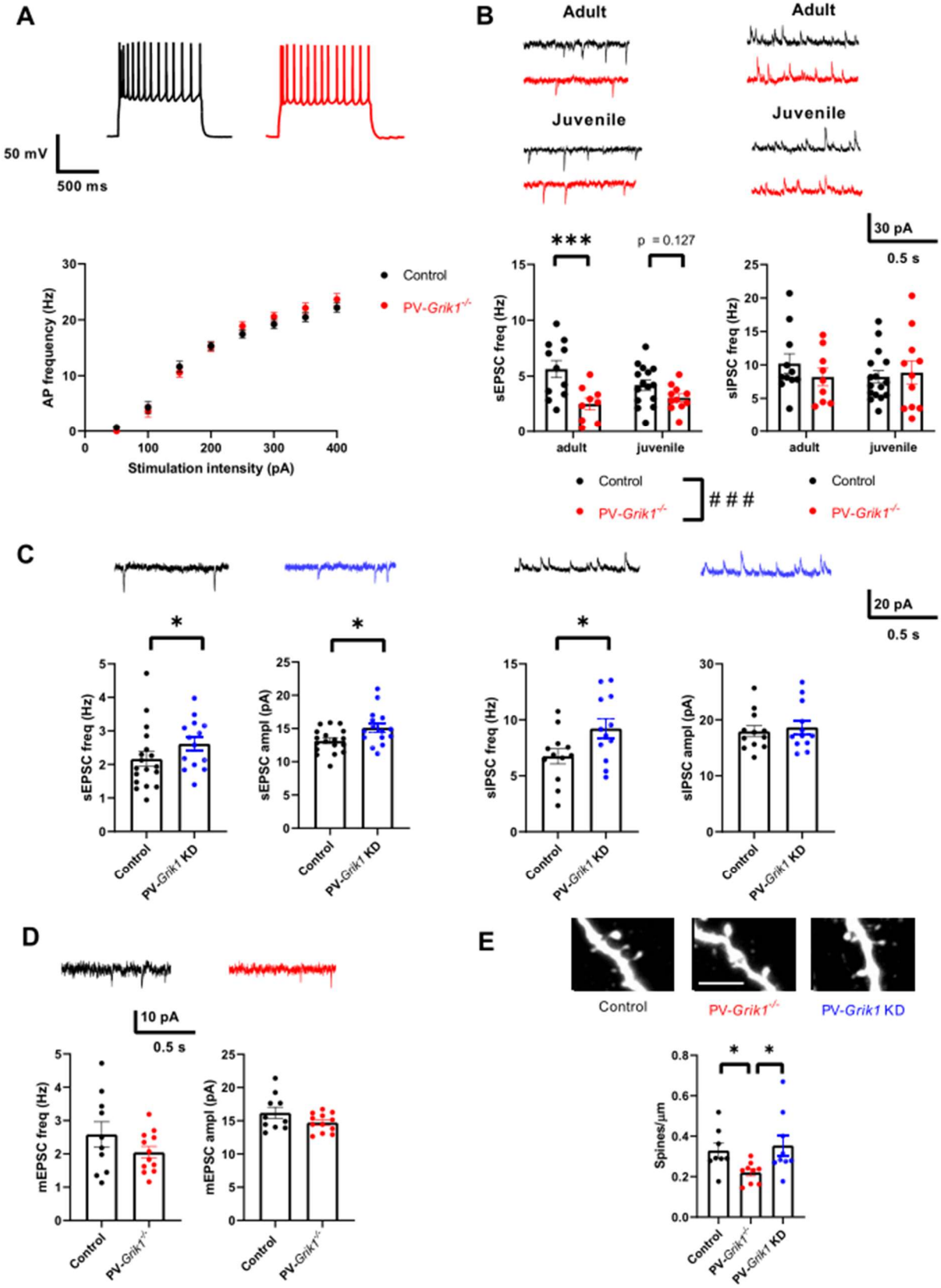
A
50 mV
500 ms
AP frequency (Hz)
Stimulation intensity (pA)
Control
PV-Grik1-/-
B
Adult
Juvenile
30 pA
0.5 s
***
p = 0.127
sEPSC freq (Hz)
sIPSC freq (Hz)
adult
juvenile
###
C
20 pA
0.5 s
*
sEPSC freq (Hz)
sEPSC ampl (pA)
sIPSC freq (Hz)
sIPSC ampl (pA)
Control
PV-Grik1 KD
D
10 pA
0.5 s
mEPSC freq (Hz)
mEPSC ampl (pA)
E
Spines/µm

Figure 5. Synaptic inputs and excitability of BLA PN's in mice lacking GluK1 in BLA PV+ interneurons. **A.** BLA neuron excitability. Example traces (top; control: black trace, *PV-Grik1*$^{-/-}$*:* red trace), as well as quantification of AP firing frequency of BLA neurons in response to depolarizing current steps (bottom). No significant differences in AP frequencies were observed when comparing control and *PV-Grik1*$^{-/-}$ mice ($F_{(1, 131)} = 0.9559$, $p = 0.33$, mixed effects model (REML)). **B**. Example traces of sEPSCs and sIPSCs, recorded from BLA PN's from both adult (n = 11 cells, 5 animals) and juvenile control (black traces) (n = 15 cells, 4 animals) and *PV-Grik1*$^{-/-}$ (red traces) mice (adult: n = 9 cells, 4 animals, juvenile: n = 18 cells, 4 animals) (top). Below, quantification of sEPSC frequency (left) and sIPSC frequency (right), ***$p < 0.001$; Holm-Sidak, ### $p < 0.001$; 2-way ANOVA. **C.** Consequences of knockdown of GluK1 from PV+ interneurons on glutamatergic and GABAergic drive onto BLA neurons**.** Example traces of sEPSCs and sIPSCs, recorded from BLA PN's from adult control and *PV-Grik1* KD groups (top) and pooled data (control sEPSC: n = 18 cells, 3 animals, control sIPSC: n = 12 cells, 3 animals, *PV-Grik1* KD sEPSC: n = 14 cells, 3 animals, *PV-Grik1* KD sIPSC: n = 12 cells, 3 animals), * $p < 0.05$; unpaired t-test ; # $p < 0.05$ Mann Whitney test. **D.** Example traces as well as quantification of mEPSC frequency and amplitude from adult control (n = 10 cells, 4 animals) and *PV-Grik1*$^{-/-}$ mice (n = 11 cells, 4 animals). **E.** Example images as well as quantification of spine density of adult BLA neurons of control (n = 8 slices, 3 animals), *PV-Grik1*$^{-/-}$ (n = 9 slices, 3 animals) and *PV-Grik1* KD (n = 9 slices, 3 animals) mice. Scale bar = 5 µm. * $p < 0.05$; one-way ANOVA.

FIGURE 6

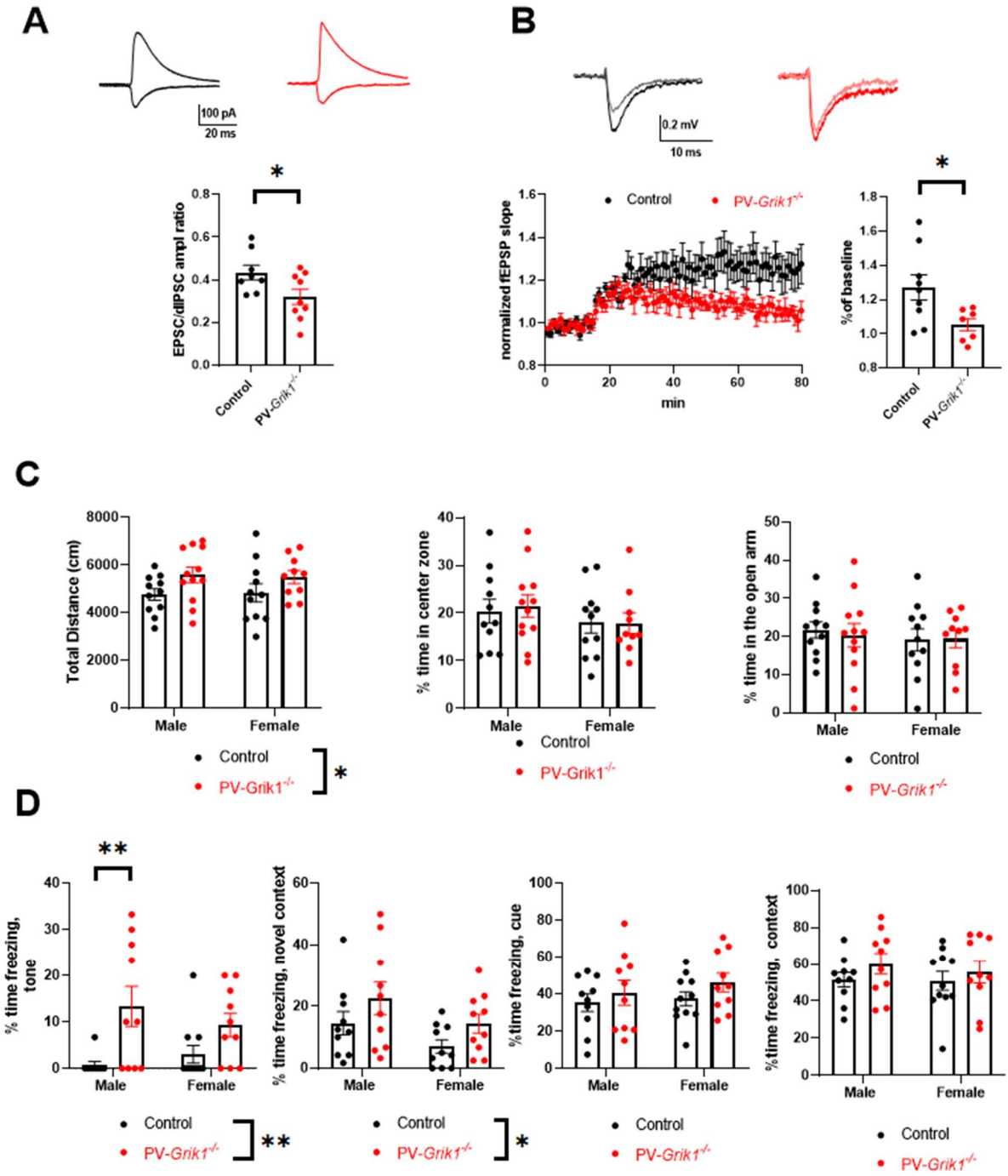

Figure 6. Absence of GluK1 in PV+ interneurons affects BLA microcircuit function and amygdala-dependent behavior. **A.** FFI at cortical inputs to BLA PNs. On the top, example traces of EPSC and dIPSC, recorded from BLA principal neuron in control and *PV-Grik1*$^{-/-}$ mouse. Traces represent the average of 5 responses. On the bottom, quantification of EPSC/dIPSC ratio (control: n = 8 cells (4 animals), *PV-Grik1*$^{-/-}$: n = 9 cells (6 animals); * $p < 0.05$, one-way ANOVA). **B.** LTP recordings. On top, example traces of fEPSPs during baseline (light gray and light red, for control and *PV-Grik1*$^{-/-}$, respectively) and after 1 hour of TBS stimulation (black and dark red, for control and *PV-Grik1*$^{-/-}$, respectively). Traces represent the average of 5 responses. TBS induced changes in synaptic strength

were significantly different between genotypes (control: n = 9 slices (4 animals), *PV-Grik1*$^{-/-}$: n = 7 slices (3 animals) * $p < 0.05$, one-way ANOVA). **C.** OF (left and middle) and EPM (right) behavioral tests in male and female *PV-Grik1*$^{-/-}$ mice with littermate controls. Total distance travelled in the OF was significantly different between the genotypes (* $p<0.05$; two-way ANOVA). No differences between the groups were detected in the % time spent in the center zone of the OF arena ($F_{(1, 40)} = 0.04091$, $p = 0.8407$, 2-way ANOVA) or in open arms in the EPM ($F_{(1, 40)} = 1.072$, $p = 0.3067$, two-way ANOVA). Control: male n = 11, female n = 11; *PV-Grik1*$^{-/-}$: male n = 12, Female n = 10. **D.** *PV-Grik1*$^{-/-}$ mice exhibit a fear of novelty. Time spent freezing during a novel tone and in novel context was significantly different between the genotypes (* $p < 0.05$ ** $p < 0.005$, two-way ANOVA with Holm-Sidak). In fear conditioning, no differences were found in time spent freezing when presented with the conditioned cue ($F_{(1, 37)} = 1.930$ $p = 0.1730$) or when placed in a novel context ($F_{(1, 37)} = 1.653$ $p = 0.2065$). Control: male n=10, female n=11; *PV-Grik1*$^{-/-}$: male n = 10, Female n = 10.